ELECTRODEPOSITION OF DIAMOND-LIKE CARBON FILMS

Minhua Chen, B.S.

Thesis Prepared for the Degree of

MASTER OF SCIENCE

UNIVERSITY OF NORTH TEXAS

August 2002

APPROVED:

Teresa D. Golden, Major Professor
Nandika A. D'Souza, Committee Member, Materials Science Department
Oliver M. R. Chyan, Committee Member
Ruthanne D. Thomas, Chair of the Department of Chemistry
C. Neal Tate, Dean of the Robert B. Toulouse School of Graduate Studies

Chen, Minhua, Electrodeposition of Diamond-like Carbon Films. Master of Science (Analytical Chemistry), August 2002, 75 pp., 5 tables, 28 illustrations, references, 65 titles.

Electrodeposition of diamond-like carbon (DLC) films was studied on different substrates using two different electrochemical methods. The first electrochemical method using a three-electrode system was studied to successfully deposit hydrogenated DLC films on Nickel, Copper and Brass substrates. The as-deposited films were characterized by scanning electron microscopy (SEM), Raman spectroscopy, X-ray photoelectron spectroscopy (XPS), fourier transform infrared spectroscopy (FTIR) and cyclic voltammetry (CV). A variety of experimental parameters were shown to affect the deposition process.

The second electrochemical method was developed for the first time to deposit hydrogen free DLC films on Ni substrates through a two-electrode system. The as-deposited films were characterized by Raman spectroscopy and FTIR. According to Raman spectra, a high fraction of diamond nanocrystals were found to form in the films.

Several possible mechanisms were discussed for each deposition method. An electrochemical method was proposed to deposit boron-doped diamond films for future work.

ACKNOWLEDGMENTS

My special thanks go to my advisor Dr. Teresa D. Golden for her continuous support and generous help. She always encourages me to think creatively and apply new ideas into research. I would also like to thank my colleagues Charoendee Pingsuthiwong and Qi Wang for their help in my research. I appreciate the Welch Foundation and UNT Faculty Research Grant for their financial support.

Finally I wish to extend my gratitude to my father Linxi Chen, my mother Fengxian Chen and my wife Suling Zhang for their continuous love and encouragement.

TABLE OF CONTENTS

LIST OF TABLES

LIST OF ILLUSTRATIONS

CHAPTER 1

INTRODUCTION

Diamond-like carbon (DLC) films have been studied for nearly three decades. The films are attractive because of the unique properties and characteristics such as high hardness, high thermal conductivity, high chemical inertness and high corrosion resistance. The deposition of DLC films has been mainly accomplished by two types of methods: chemical vapor deposition (CVD) and physical vapor deposition (PVD). While there has been much study on CVD [1-6] and PVD of DLC films [7-10], the disadvantages of these technologies are clear given the requirement of high voltage, high vacuum and therefore high cost. Electrodeposition offers us a novel route of synthesis for DLC films. Since the first electrodeposition study of Namba [11] in 1992, the electrodeposition of DLC films have been investigated by several research groups [12-27]. The electrodeposition methods, compared with CVD and PVD, have demonstrated some obvious advantages in terms of simple setup, low temperature and low cost. However, all of the previous work involved the use of high potential, operating at low temperature with a high potential difference between the anode and cathode. Thus their electrodeposition methods, although operated under low temperature, involve the use of high electric field due to the high potential difference between the anode and cathode.

The only report of electrodepositing DLC films at both low temperature and low potential was done by V.P.Novikov et al. [28] in 1996, simplifying the setup and making it possible to study the probable deposition mechanism. However, V.P.Novikov et al.'s reports [28-31] were vague leaving unexplored such things as use of different substrates

and changing of parameters on the deposition of DLC films. Much more studies need to be conducted to explore this method in further details. To explore the feasibility, reliability and the potential of using electrochemical methods to deposit diamond-like carbon films on different substrates, this thesis includes the following information. In the first chapter, based on the method by V. P. Novikov et al. [28], an electrochemical cell, composed of a working electrode (WE), counter electrode (CE) and reference electrode (RE), was used to deposit DLC films on different substrates, including Ni, Cu, Brass, Stainless Steel, Co and Mo. In the second chapter, an electrochemical cell consisting of WE and CE was developed for the first time to deposit DLC films on Ni substrates with DC power as the source. Lastly, based on the results of the first and second sections, an electrochemical method was proposed to deposit boron-doped diamond films.

1.1. What are Diamond-like Carbon Films?

Carbon is unique among all the elements. Two pure carbon crystalline forms, graphite (sp^2, threefold planar bonding), and diamond (sp^3, fourfold tetrahedral bonding) have been known and used for centuries along with other less clearly identified carbon materials (‘coals’) [32]. Diamond-like carbon (DLC) film is a form of carbon produced for the first time in 1969 by Aisenberg and Chabot [33, 34]. They sputtered carbon electrodes in an argon plasma and used the carbon ions for deposition of transparent, hard and insulating carbon films. These carbon films had most of the properties of natural diamond but were predominantly amorphous and not crystalline. So “diamond-like” was used to identify the properties of the produced material. After that, a variety of deposition methods employing

energetic species were used to deposit DLC films. DLC films can be divided into two types [32]: hydrogen free DLC or hydrogenated DLC. Nomenclatures such as 'a-C:H' (amorphous carbon hydrogenated), 'HDLC' (hydrogenated DLC) and 'DLHC' (diamond-like hydrocarbon) are often used to label hydrogenated DLC. In some papers, DLC films without mentioning hydrogen content is also labeled as hydrogenated DLC. A predominantly sp^3 film ($sp^3 > 70\%$) with a tetrahedral local carbon configuration is denoted as ta-C. In this thesis, DLC represents both hydrogenated DLC and hydrogen free DLC.

1.1.1. Structure

All DLC films are substantially amorphous, but some micro or nano-crystalline inclusions of all carbon forms can be found in the amorphous matrix. The utmost layer of DLC films is porous and defective and its sp^2 fraction is close to 100%, much higher than the sp^3 rich material underneath. These defective layers strongly affect the surface related properties of DLC films. The structure of DLC films can be divided into two categories: (I). Substantially tetrahedral but containing sp^2 bonded carbon, (II). Substantially three folded but containing sp^3 bonded atoms.

1.1.2. Properties and Application

DLC films feature a unique set of properties including:

1. High hardness and wear resistance
2. High optical transparency
3. High electrical resistance and dielectric strength

4. Good thermal conductivity

5. High chemical inertness

6. High corrosion resistance

7. Low friction coefficient

8. Bio-compatibility

Due to the above properties, DLC can be applied into electronics and optics as wear-resistant coatings, infrared optical coatings, integrated circuit passivation coatings, and biocompatible coatings.

1.2. Physical Vapor Deposition and Chemical Vapor Deposition of DLC Films

Vapor deposition refers to any process in which materials in a vapor state are condensed through condensation, chemical reaction, or conversion to form a solid material. These processes are used to form films on different substrates. Vapor deposition processes usually take place within a vacuum chamber. It can be divided into two categories: chemical vapor deposition (CVD) and physical vapor deposition (PVD).

In CVD, thermal energy heats a volatile precursor (vapor or gas) in the coating chamber and drives the deposition reaction. A film is formed on a surface as a consequence of one or more chemical reactions which change the state of the precursor. Many different films can be deposited: elements and compounds, crystalline, polycrystalline, and amorphous. Most films can be deposited from several different precursor systems. Plasma discharges can be used to increase the discharge deposition rates, or the substrate and/or the gas can be heated or cooled. Different deposition

techniques, process conditions, and treatment after deposition produce films with varying characteristics, suitable for different applications. Each film has an optimal set of characterization techniques. Nevertheless, in every case, CVD processes must provide a volatile precursor containing the constituents of the film, transport that precursor to the deposition surface, avoid reactions in the gas phase, encourage surface reactions that form the film and proceed it rapidly, reproducibly, and uniformly for industrial applications.

In PVD, the material in solid form is either heated until evaporation (thermal evaporation) or sputtered by ions (sputtering). Then the vapor of the material will be deposited on the target substrate surface as a thin film. In sputtering, ions are generated by a plasma discharge usually within an inert gas (argon). It is also possible to bombard the sample with an ion beam from an external ion source. This allows the energy and intensity of ions to vary reaching the target surface. Alternatively, it is possible to use the ion source to directly bombard the substrate surface during the evaporation process, to impart a higher energy to the evaporated atoms and achieve a film with better properties (adherence, density, etc.). This technique, called “ion beam assisted deposition”, is also available and has been conveniently used to deposit carbon films (DLC) and binary and ternary compounds of the carbon-boron-nitrogen family.

CVD and PVD, as traditional technologies, are widely used to produce DLC films [1-10]. For DLC films, the carbon source is an ionized carbon containing gas (e.g. CO, CO_2 or hydrocarbon gas) in CVD and a pure carbon target in PVD. A variety of diamond films, hydrogenated DLC films and hydrogen free DLC films have been produced using vapor

deposition technologies. Both CVD and PVD feature some advantages in that they can provide high rapid growth rate, good adhesion, uniform thickness and the technologies are well developed. However, the high vacuum required in the vapor deposition makes the equipment rather complicated and the control of the experiments difficult. The comparatively high process temperature (e.g. approx. 200-500 ^{o}C for PVD, 600-1000 ^{o}C for CVD) also limits their application on low melting substrates such as plastics.

The disadvantages in vapor deposition present a need for an additional technology to be developed.

1.3. Electrochemical Methods

Although high quality and rapid growth rates are achieved in the traditional technologies applied for DLC films, the high substrate temperature as well as the complex equipment have limited their application.

In 1992, Namba [11] first employed electrochemical methods to deposit DLC films. In his study, diamond phase carbon films had been grown on silicon substrates at temperatures of less than 70 ºC by using ethanol solution. The potential applied to silicon substrates was changed from 0 to -1.2 KV and the current density from 0 to 5 mA/cm^2. By changing the electrolyte into a water-ethylene glycol solution, Suzuki et al. [12] soon successfully deposited carbon films on the silicon substrate. After that, this electrolysis method had been successfully employed to deposit DLC films from a variety of organic solution including methanol, acetonitrile, N, N-dimethylformamide, nitromethane, nitroethane, ethanol and acrylonitrile [14-26]. Both DC power and pulse-modulated power

were used as energy sources in these attempts. In 1996, Suzuki et al. [13] reported a new approach to deposit carbon films from organic solutions by electrolytic heating of a water-ethanol solution. This method consisted of discharge-heating a tungsten cathode in a water-ethanol electrolyte under a high DC voltage. At high voltages, glassy carbon and disordered graphitic carbon were deposited on the tungsten wire. Very similarly, Wang et al. [27] has employed a thin tungsten wire as anode under high potential and successfully deposited DLC films on silicon substrates. All of the above electrochemical methods have demonstrated some obvious advantages over traditional PVD and CVD in terms of low processing temperature, simple setup and low cost. However, all of them involved the use of high potential, which greatly increases the difficulty to control the deposition process and study the mechanism. In 1996, V. P. Novikov et al. [28] proposed a new electrochemical method to deposit DLC films. They used a solution of acetylene in liquid ammonia as electrolyte and carried out the electrolysis at a low voltage of 2.5 to 5 V as well as low temperature -55 ^{o}C. In their study, a diamond phase peak and a graphite peak were respectively observed in Raman spectra. This method, processed at both low potential and low temperature, has further simplified the setup and made it possible to control the deposition process by charge and study the probable deposition mechanism. However, V. P. Novikov et al.'s reports [28-31] left many things unexplored such as application to different substrates, the effects of different parameters on the deposition of DLC films and the potential to deposit other thin films. More studies need to be conducted to explore this method in further details.

1.4. Characterization of Diamond-like Carbon Films

A variety of analysis methods are used to characterize the DLC films. Most of them focus on phase determination, that is, evaluation of the sp^3 fraction of the films. Other methods are employed to probe the optical, electrical, mechanical, tribological and morphology properties. The techniques most frequently used for phase determination of DLC films include surface analysis [Auger electron spectroscopy (AES), X-ray photoelectron spectroscopy (XPS), low energy electron energy loss spectroscopy (EELS)], high energy EELS, diffraction and radial distribution function (RDF) analysis via electron (using a transmission electron microscope, TEM) or neutron scattering studies, and Raman microscopy or spectroscopy. Atomic force microscopy (AFM) and scanning electron microscopy (SEM) were shown to accurately measure the surface morphology of DLC films. The optical properties of DLC films may be obtained by either transmission measurements, when deposited on transparent substrates, or by reflection measurements, when deposited on non-transparent substrates, when ellipsometry is used. Fourier Transform Infrared Spectroscopy (FTIR) is used to probe the hydrogen information in the DLC films. Hardness measurements and Young's Modulus can be determined using indentation or nanoindentation techniques. Novel ultrasonic surface wave technique can also be used to determine the Young's Modulus. In this study, Raman spectroscopy, XPS, FTIR and SEM are the main analysis methods to characterize DLC films. Detailed information about these techniques follows below.

1.4.1. Raman Spectroscopy

Before we discuss the application of Raman spectroscopy in DLC films, let us first recall the basics of Raman spectroscopy.

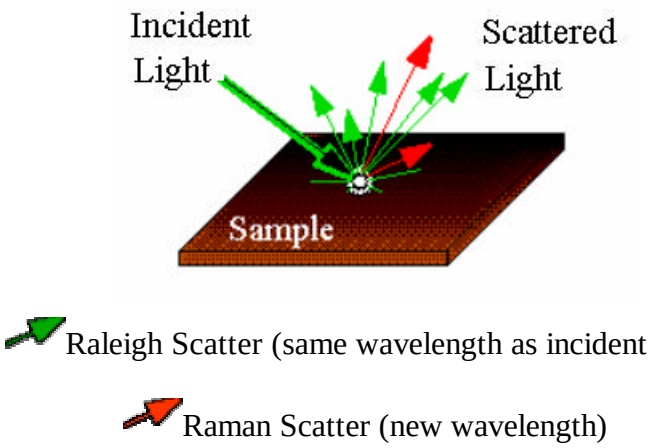

Figure 1.1. Schematic illustration of Raman effect

The Raman effect arises when the incident light excites molecules in the sample that subsequently scatter the light. While most of this scattered light is at the same wavelength as the incident light, some is scattered at a different wavelength. This inelastically scattered light is called Raman scatter. It results from the molecule changing its molecular motions. Those energy levels found below the incident frequency are traditionally called Stokes frequencies, while those scattered above the original frequency are called anti-Stokes. Since the original population of molecular energy levels follows a Boltzmann distribution, the intensity of the Stokes frequencies is expected to be much greater than that of the anti-Stokes. In practice, observed Raman spectra are almost always the Stokes lines. The energy difference between the incident light (Ei) and the Raman scattered light (Es) is equal to the

energy involved in changing the molecule's vibrational state. This energy difference is called the Raman shift.

$Ev = Ei - Es$

Several different Raman shifted signals are often observed, each being associated with different vibrational or rotational motions of molecules in the sample. The particular molecule and its environment will determine what Raman signals will be observed. A plot of Raman intensity vs. Raman shift is a Raman spectrum.

Raman spectroscopy is probably the most common technique used for evaluation of carbon films because of its ability to distinguish between different forms of carbon. For diamond, the single phonon (first order) Raman spectra produced using laser excitation in the visible range (e.g. 514.5 nm from the Ar^+ ion lasers) gives a single band at 1332 cm^{-1}. Generally, Raman scattering immediately above the diamond one-phonon band is assigned to sp^2 carbon containing materials. Three generally distinguishable types of sp^2 carbon include: crystalline graphite (a single band at 1580 cm^{-1}), defective or microcrystalline graphite (two broad bands at ca. 1580 and 1350 cm^{-1}), and amorphous carbon (a broad asymmetric band peak at around 1500 ± 40 cm^{-1}).

For DLC films, although it contains both sp^3 and sp^2 carbon, no 1332 cm^{-1} Raman band is detected. This is due to the much higher sensitivity (by a factor of 50) to sp^2 bonding with respect to sp^3 bonding. Overall, two typical Raman peaks are detected at around 1350 cm^{-1} (called D peak) and 1580 cm^{-1} (called G peak) respectively for DLC films. The G peak is attributed to the graphite-like layers of sp^2 micro domains, while the D peak is due

to the bond-angle disorder in the sp^2 graphite-like micro domains induced by the linking with sp^3-C atoms as well as the finite crystalline sizes of sp^2 micro domains [35-37].

Tuinstra et al. [35] established a linear relationship between the ratio of integrated intensities of the D and G peaks (I_D/I_G) and inverse crystallite size ($1/L_a$, where L_a is the crystallite size) with the aid of x-ray diffraction. Knight [15] concluded that I_D/I_G was inversely proportional to the L_a, for 2.5 nm < L_a < 300 nm. Prawer et al. [14] has found that the I_D/I_G increased from about zero to 1.8 as the size of the crystallites increased from effectively zero to about 2.5 nm. During the study on annealed carbon, Dillon et al. [37] have found I_D/I_G was proportional to the crystallite number or size at the lower temperature range and inversely proportional to the size and dimensions of crystallites at higher temperature range. Therefore, as yet, a consistent relationship between I_D/I_G and crystallites has not been determined.

Prawer et al. [38] proposed that Raman spectroscopy could be used to identify the microstructure of hydrogen free DLC films by fitting the Raman spectrum with Breit-Wigner-Fano (BWF) lineshape [39]. If the fit does not show a residual in the region of about 1350 cm^{-1} (i.e. the D peak), the sp^2 component of the film is likely to be less than 20%. The BWF lineshape is quite symmetric for films with low sp^2 content and highly asymmetrical for films with high sp^3 content. Also the peak position decreases as a function of the sp^2 content. In addition, Ultraviolet (UV) Raman was proved to be capable of resonantly enhancing the sensitivity to sp^3 bonding with respect to sp^2 thus revealing the broad line below 1300 cm^{-1} expected for an amorphous sp^3 bonded carbon [32].

In conclusion to this section, let us summarize the application of Raman spectroscopy in DLC films again. First DLC films feature two typical Raman peaks at around 1350 cm^{-1} and 1580 cm^{-1}, the D peak and G peak respectively. No sp^3 carbon peak can be detected directly due to the much lower sensitivity of Raman to sp^3 carbon with respect to sp^2 carbon. The I_D/I_G can be used to provide the size information of finite sp^2 graphite crystallites. By fitting the Raman peak with a single skewed lorentzian, limited information about sp^3 composition can be obtained. Besides the D peak and G peak, other peaks exist in the Raman spectra of DLC films due to the complicated structure of DLC films. For example, a peak at around 1230 cm^{-1} was found in the Raman spectra of DLC films by Gonon et al. [40], Popovici et al. [41] as well as my research. This peak is assigned to diamond nanocrystals in the DLC films. Finally, one thing has to be kept in mind when dealing with DLC films, that is, DLC films are not a mixture of distinct features typical of graphite and diamond, but a new structure with both sp^3 four-coordinated carbon and sp^2 three-coordinated carbon, that are complicatedly bonded [36].

1.4.2. X-ray Photoelectron Spectroscopy (XPS) / Electron Spectroscopy for Chemical Analysis (ESCA)

XPS, also called ESCA, was developed in the mid 1960s by K. Siegbahn and his research group. K. Siegbahn was awarded the Nobel Prize for Physics in 1981 for his work in XPS. The phenomenon is based on the photoelectric effect outlined by Einstein in 1905 where the concept of the photon was used to describe the ejection of electrons from a surface where photons impinge upon it.

For XPS, Al K_a (1486.6eV) or Mg K_a (1253.6eV) is often the photon energies of choice. Other X-ray lines can also be chosen such as Ti K_a (2040eV). These soft X-rays ionize atoms in a solid and the energies of emitted photoelectrons from core shells in the atom (photoelectric effect) are analyzed. The difference between the X-ray energy and the photoelectron energies gives the binding energies (BEs) of the core level electrons, an atomic characteristic. The peak areas can be used (with appropriate sensitivity factors) to determine the composition of the materials surface. The shape of each peak and the binding energy can be slightly altered by the chemical state of the emitting atom. Hence XPS can provide chemical bonding information as well. The low kinetic energy (by definition < 1.5 keV) of photoelectrons makes XPS inherently surface sensitive with the majority of the photoelectrons in a given sample originating from the outer 5 nm. XPS is not sensitive to hydrogen or helium, but can detect all other elements.

XPS must be carried out in ultra high vacuum (UHV) conditions. UHV conditions are generally regarded as being in the region below 10^{-9} millibar. Since atmospheric pressure is about 1 bar, this means that the number of atoms of gas in a UHV chamber is 1/1,000,000,000,000 that of air per unit volume. Frequently pressures are a factor 10 or more below this. UHV is needed for surface science as molecules in an atmosphere will land on a surface and change its properties. Even at a pressure of 10^{-6} millibar, a layer of gas atoms will form on the surface in about 3 seconds (assuming every atom to strike the surface sticks to the surface). This is clearly not enough time to do an experiment. However, at UHV pressures, which are a factor 1000 and more lower in pressure, means that hours are needed before the sample is significantly degraded. In order to achieve

UHV, some special procedures are needed. Initially, the vacuum chamber will be pumped down to 10^{-2} millibar using a rotary pump. Then the chamber will be pumped down to about 10^{-6} millibar with a turbomolecular pump. At this stage, the vacuum chamber is enclosed in heat resistant boards (known as ovens), and baked to a temperature of about 180 ^{o}C. After a day or so of baking, the ovens are removed, and the chamber allowed to cool down again. Once down at room temperature, the chamber should have a pressure in the UHV region. The process of baking removes gas atoms which are stuck to the chamber walls. These gas atoms slowly desorb from the chamber wall surfaces, and if the chamber was not baked, then months would pass before the chamber achieved UHV conditions.

In the study of DLC films, XPS is mainly utilized to obtain the elemental composition and a quantitative characterization of the fraction of sp^3 carbon and sp^2 carbon at the surface of the films. First, all elements except hydrogen or helium can be detected by XPS. Furthermore, by focusing on the C1s, detailed information about sp^3 and sp^2 carbon can be obtained. Due to the difference of the local environment, the binding energy of sp^3 is slightly higher than that of sp^2 carbon, which, shown in XPS, is an asymmetric XPS peak or overlapped peak for C1s. By using gaussian-curve fitting procedure, it can be deconvoluted into two separate peaks with higher peak corresponding to sp^3 carbon and lower peak due to sp^2 carbon.

1.4.3. Fourier Transform Infrared Spectroscopy (FTIR)

Fourier Transform Infrared Spectroscopy (FTIR) is an analytical technique used to identify organic materials. This technique measures the absorption of various infrared light wavelengths by the material of interest. These infrared absorption bands identify specific molecular components and structures.

Absorption bands in the range of 4000 - 1500 wavenumbers are typically due to functional groups present on the molecules (e.g. -OH, C=O, N-H, CH_3, etc.). The region between 1500 - 400 wavenumbers is referred to as the fingerprint region. Absorption bands in this region are generally due to intra-molecular phenomena, and are highly specific for each material. The specificity of these bands allows computerized data searches to be performed against reference libraries to identify a material. To determine the identity of the material being analyzed, the unknown IR absorption spectrum is compared with standard spectra in computer databases or a spectrum obtained from a known material. Matches identify the polymer or other organic constituent(s) in the sample. In addition, FTIR can also be used to quantify a material. Quantitative concentration of a compound can be determined from the area under the curve in characteristic regions of the IR spectrum. Concentration calibration is obtained by establishing a standard curve from spectra for samples of known concentrations.

As far as DLC films are concerned, FTIR is an effective tool in analyzing the hydrogen content and probing the different C-H configuration by using the reflectance mode of the microscope. As for aliphatic hydrocarbons, C-H stretching vibrations occur in the region 2975-2840 cm^{-1} for hydrogenated DLC films [44]. The CH_3 asymmetric stretching vibration occurs at 2975-2950 cm^{-1} and may be easily distinguished from the nearby CH_2

absorption at about 2930 cm^{-1}. The symmetric CH_3 stretching absorption band occurs at 2885-2865 cm^{-1}, and that of CH_2 at 2870-2840 cm^{-1}.

1.4.4. Scanning Electron Microscopy (SEM)

Scanning Electron Microscopy (SEM) uses a focused electron beam to scan small areas of solid samples. Secondary electrons are emitted from the sample and are collected to create an area map of the secondary emissions. Since the intensity of secondary emission is very dependent on local morphology, the area map is a magnified image of the sample. Spatial resolution is as high as 1 nm for some instruments, but 4 nm is typical for most. Magnification factors can exceed 500,000. Backscattered electrons (BSE) and characteristic X-rays are also generated by the scanning beam and many instruments can utilize these signals for compositional analysis of microscopically small portions of the sample. Energy Dispersive Spectroscopy (EDS) is such a standard procedure by using the characteristic X-rays for identifying and quantifying elemental composition of sample areas as small as a few cubic micrometers. In SEM, the characteristic X-rays are produced when a material is bombarded with electrons in an electron beam instrument. Detection of these x-rays can be accomplished by an energy dispersive spectrometer, which is a solid state device that discriminates among X-ray energies.

For DLC films, SEM is mainly used to probe the morphology of the surface and measure the thickness of the thin films. With EDS attached to SEM, elemental composition information can also be obtained.

1.5. Liquid Ammonia System

Liquid ammonia is of interest in electrochemistry because of its excellent solvent power, its relatively high dielectric constant and low viscosity and the extraordinary properties of metal-ammonia solutions. Many different types of reactions can be carried out using liquid ammonia as a reaction medium [42, 43]. When applied into electrochemical reaction as reaction medium, two properties of liquid ammonia are important: thermodynamic stability and conductivity. As for thermodynamic stability, liquid ammonia can be electrolytically decomposed into nitrogen at the anode and hydrogen at the cathode with a very low theoretical decomposition voltage (0.076 V at -34 ^{o}C) [45]. This means that the range of thermodynamic stability is very narrow and that little potentiality for oxidations and reductions should be expected between the two limiting reactions:

$6NH_2^-$? $N_2 + 4\ NH_3 + 6e^-$ at the anode

$2NH_4^+$? $H_2 + 2\ NH_3 - 2e^-$ at the cathode

Fortunately, the overvoltage connected with these processes are so high that on smooth platinum electrodes the actual decomposition voltage is of the order of 3 V at –34 ^{o}C. There are, therefore, still many possibilities for chemical and electrochemical oxidations and reductions outside the field of thermodynamic stability.

The conductance of highly purified liquid ammonia can be as low as 10^{-11} ? $^{-1}cm^{-1}$ at -34 ^{o}C [46]. Under ordinary conditions, obtained ammonia has a conductance on the order of about 10^{-7} ? $^{-1}cm^{-1}$. In electrochemical studies, such a low conductance is a big obstacle for electrochemical current. Therefore, a supporting electrolyte such as KI [43] is often

added into liquid ammonia. The dissociation of KI in liquid ammonia provides sufficient ions to transport electrical charge during the electrochemical reaction. However, careful consideration has to be given when selecting the supporting electrolyte involved in the electrochemical experiement. In our study, acetylene was saturated with liquid ammonia as electrolyte. Conductometric measurements made by Masdupuy [47] on liquid ammonia saturated with acetylene at -42 ^{o}C have given a value of 0.00073 ? $^{-1}$cm^{2} for the molar conductance of this solution. To increase the conductance, sodium acetylide was added as the supporting electrolyte. Sodium acetylide is a weak electrolyte in liquid ammonium. In general, for this weak electrolyte, there is a limiting equivalent conductance, which is 262 ? $^{-1}$cm^{2}. When the solution of sodium acetylide in liquid ammonia is infinitely diluted, this limiting conductance can be reached. In other words, the conductance increases as the concentration of sodium acetylide decreases. An experimental conductance values for sodium acetylide obtained by Bombara et al. [48] is given in Tables 1.1.

Table 1.1. Experimental conductance for sodium acetylide in liquid ammonia

C(moles/l)	2.80× 10^{-5}	1.810× 10^{-4}	3.52× 10^{-4}	1.75× 10^{-3}	8.64× 10^{-3}	1.80× 10^{-2}	6.51× 10^{-2}	1.04× 10^{-1}
? (? $^{-1}$cm^{2})	246.2	212.7	181.8	116.8	63.7	51.0	32.0	31.8

A method to prepare pure liquid ammonia was given by Giuseppe et al. [20]. All of the above discussions are based on highly purified liquid ammonia. However, many sources of contamination can easily increase the conductance of liquid ammonia. The purification of

liquid ammonia depends on the specific needs of experiments. In this study, a highly purified liquid ammonia is not required, on the contrary, the existing of some impurity in the liquid ammonia makes it possible to obtain a higher conductance without adding any supporting electrolytes.

References

1. H. Buchkremer-Hermanns, H. Ren and H. Wei, A Combined MW/ECR-PACVD Apparatus for the Deposition of Diamond and Other Hard Coatings, Surface and Coatings Technology, 74 (**1995**) 215.
2. A. Dehbi-Alaoui and A. Matthews, Diamond-like Carbon Films Grown in a New Configuration for Filament Enhanced Plasma Assisted CVD, Vacuum, 46 (**1995**) 1305.
3. K. Kuramoto, Y. Domoto, H. Hirano, S. Kiyama and S. Tsuda, High Quality Diamond Like Carbon Thin Films Fabricated by ECR Plasma CVD, Applied Surface Science, 113 (**1997**) 227.
4. D. S. Patil, K. Ramachandran, N. Venkatramani, M. Pandey, S. Venkateswaran and R. D'Cunha, Microwave Plasma Chemical Vapour Deposition of Diamond Like Carbon Thin Films, Journal of Alloys and Compounds, 278 (**1998**) 130.
5. C. Meunier, E. Tomasella, S. Vives and S. Mikhailov, X-Ray Reflectometry Study of Diamond-like Carbon Films Obtained by Plasma-enhanced Chemical Vapor Deposition, Diamond and Related Materials, 10 (**2001**) 1491.
6. M. Ban, M. Ryoji, T. Hasegawa, Y. Mori, S. Fujii and J. Fujjoka, Diamond-like Carbon Films Deposited by Electron Beam Excited Plasma Chemical Vapor Deposition, Diamond and Related Materials, 11 (**2002**) 1353.
7. H. Kaufmann, Industrial Applications of Plasma and Ion Surface Engineering, Surface and Coatings Technology, 74 (**1995**) 23.

8. H. J. Scheibe, B. Schultrich, R. Wilberg and M. Falz, Laser-Arc Technology for Industrial Hard Coating Deposition, Surface and Coatings Technology, 97 (**1997**) 410.
9. D. Wang, C. Chang and W. Ho, Characterization of Hydrogen-free Diamond-like Carbon Films Deposited by Pulsed Plasma Technology, Thin Solid Films, 355 (**1999**) 246.
10. D. Yang, C. Chang and W. Ho, Oxidation Behavior of Diamond-like Carbon Films, Surface and Coatings Technology, 120 (**1999**) 138.
11. Y.Namba, Attempt to Grow Diamond Phase Carbon Films from an Organic Solution, J. Vac. Sci. Technol., A 10 (**1992**) 3368.
12. T. Suzuki, Y. Manita, T. Yamazaki, S. Wada and T. Noma, Deposition of Carbon Films by Electrolysis of a Water-ethylene Glycol Solution, Journal of Materials Science, 30 (**1995**) 2067.
13. T. Suzuki, T.Noma, S.Wada, T. Yamazaki, Y. Manita and T. Yanai, Carbon Deposition by Electrolytic Heating of a Water-ethanol Solution, Journal of Materials Science, 31 (**1996**) 3743.
14. H. Wang, M.Shen, Z. Ning, C. Ye, C. Cao, H. Dang and H. Zhu, Deposition of Diamond-like Carbon Films by Electrolysis of Methanol Solution, Appl. Phys. Lett., 69 (**1996**) 1074.
15. H. Wang, M. Shen, Z. Ning, C. Ye and H. Zhu, Pulsed Electrodeposition of Diamond-like Carbon Films, J. Mater. Res., 12 (**1997**) 3102.

16. J. Jiu, K. Cai, Q. Fu, C. Cao and H. Zhu, Liquid Deposition of Hydrogenated Carbon Films in N, N-dimethyl formamide solution, Materials Letters, 41 (**1999**) 63.
17. Q. Fu, J. Jiu, H. Wang, C. Cao and H. Zhu, Simultaneous Formation of Diamond-like Carbon and Carbon Nitride Films in the Electrodeposition of an Organic Liquid, Chemical Physics Letters, 301 (**1999**) 87-90.
18. J. Jiu, H. Wang, K. Cai, Q. Fu, C. Cao and H. Zhu, Liquid Phase Deposition of Hydrogenated Diamond-like Carbon Films on Conductive Glass Substrates Using a Pulse-modulated Source, Materials Research Bulletin, 34 (**1999**) 1501.
19. J. Jiu, H. Wang, C. Cao and H. Zhu, The Effect of Annealing Temperature on the Structure of Diamond-like Carbon Films by Electrodeposition Technique, Journal of Materials Science, 34 (**1999**) 5205.
20. Q. Fu, J. Jiu, C. Cao, H. Wang and H. Zhu, Electrodeposition of Carbon Films from Various Organic Liquids, Surface and Coatings Technology, 124 (**2000**) 196.
21. H. Wang, H. Kiyota, T. Miyo, K. Kitaguchi, T. Shiga, T. Kurosu, H. Zhu and M. Iida, Amorphous Carbon and Carbon Nitride Films Synthesized by Electrolysis of Nitrogen-containing Liquid, Diamond and Related Materials, 9 (**2000**) 1307.
22. C. Cao, H. Zhu and H. Wang, Electrodeposition Diamond-like Carbon Films from Organic Liquids, Thin Solid Films, 368 (**2000**) 203.
23. D. Guo, K. Cai, L. Li and H. Zhu, Preparation of Hydrogenated Diamond-like Carbon Films on Conductive Glass from an Organic Liquid Using Pulsed Power, Chemical Physics Letters, 325 (**2000**) 499.

24. K. Cai, D. Guo, Y. Huang and H. Zhu, Electrodeposition of Diamond-like Amorphous Carbon Films on Aluminum from Acetonitrile, Appl. Phys., A 71 (**2000**) 227.

25. K. Cai, D. Guo, Y. Huang and H. Zhu, Evaluation of Diamond-like Carbon Films Deposited on Conductive Glass from Organic Liquids Using Pulsed Current, Surface and Coatings Technology, 130 (**2000**) 266.

26. D. Guo, K. Cai, L. Li, Y. Huang, Z. Gui and H. Zhu, Electrodeposition of Diamond-like Carbon Films on Si from N, N-dimethylformamide, Chemical Physics Letters, 329 (**2000**) 346.

27. H. Wang and M. Yoshimura, Electrodeposition of Diamond-like Carbon Films in Organic Solvents Using a Thin Wire Anode, Chemical Physics Letters, 348 (**2001**) 7.

28. V. P. Novikov and V. P. Dymont, Synthesis of Diamond-like Phases of Carbon by an Electrochemical Method, Tech. Phys. Lett., 22 (**1996**) 283.

29. V. P. Novikov and V. P. Dymont, Synthesis of Diamondlike Films by an Electrochemical Method at Atmosphere Pressure and Low Temperature, Appl. Phys. Lett., 70 (**1997**) 200.

30. V. P. Novikov and V. P. Dymont, Mechanism of Electrochemical Synthesis of Diamond-like Carbon, Tech. Phys. Lett., 23 (**1997**) 350.

31. V. P. Dymont, M. P. Samtsov and E. M. Nekrashevich, Effect of Thermal Annealing on Spectral Properties of Electrodeposited Carbon Films, Technical Physics, 45 (**2000**) 905.

32. Y. Lifshitz, Diamond-like Carbon - Present Status, Diamond and Related Materials, 8 (**1999**) 1659.

33. S. Aisenberg and R. Chabot, J. Appl. Phys., 42 (**1971**) 2953.

34. S. Aisenberg and F. M. Kimoc, Properties and Characterization of Amorphous Carbon Films, Mater. Sci. Forum., 52-53 (**1990**) 1.

35. F. Tuinstra and J. L. Koenig, Chem. Phys., 53 (**1970**) 1126.

36. D. Beeman, J. Silverman, R. Lynds and M. R. Anderson, Modeling Studies of Amorphous Carbon, Phys. Rev. B 30 (**1984**) 870.

37. R. O. Dillon and J. A. Woollam, Use of Raman Scattering to Investigate Disorder and Crystallite Formation in As-deposited and Annealed Carbon Films, Phys. Rev. B 29 (**1984**) 3482.

38. S. Prawer, K. W. Nugent, Y. Lifshitz, G. D. Lempert, E. Grossman, J. Kulik, I. Avigal and R. Kalish, Systematic Variation of the Raman Spectra of DLC films as a Function of sp^2:sp^3 Composition, Diamond and Related Materials, 5 (**1996**) 433.

39. M. Yoshikawa, Mater. Sci. Forum, 52 (**1989**) 365

40. P. Gonon, E. Gheeraert, A. Deneuvile, F. Fontaine, L. Abello, G. Luazeau, J. Appl. Phys., 12 (**1995**) 7509

41. Galina. Popovici, C. H. Chao, M. A. Prelas, E. J. Charlson, J. M. Meese, J. Mater. Res., 10 (**1996**) 2011.

42. A. Demortier and A. J. Bard, Electrochemical Reactions of Organic Compounds in Liquid Ammonia. I. Reduction of Benzophenone, J. Am. Chem. Soc., 95 (**1973**) 3495.

43. F. A. Uribe, P. R. Sharp and A. J. Bard, Electrochemistry in Liquid Ammonia Part VI. Reduction of Carbon Monoxide, J. Electroanal. Chem., 152 (**1983**) 173.

44. George Socrates, Infrared Characteristics Group Frequencies, 2nd edition. (**1994**) 35.

45. S. Makishima, J. Fac. Eng., Univ. Tokyo., 21 (**1938**) 115.

46. V. F. Hnizda and C. A. Kraus, J. Am. Chem. Soc., 71 (**1949**) 1566.

47. E. Masdupuy, Ann. Chim. (Paris). 13a serie (**1957**) 549.

48. G. Bombara and M. Troyli, Conductometry in Liquid Ammonia I. Dissociation Constants of Sodium Acetylide and Sodium Methylbutynolate, J. Electroanal. Chem., 5 (**1963**) 379.

CHAPTER 2

ELECTRODEPOSITION OF DLC FILMS USING A THREE-ELECTRODE SYSTEM

2.1. Introduction

As introduced in Chapter 1, in 1996, for the first time V. P. Novikov et al. [28] developed a new electrochemical method to deposit DLC films on various metals at both low temperature and low potential. They used a solution of acetylene in liquid ammonia as the electrolyte. The electrolysis was carried out at a voltage of 2.5 to 5 V and the current density was 10^{-3} to 10^{-5} A/cm^2. By this method, diamond phase and amorphous carbon films were both formed according to the Raman spectra. This method, processed at both low potential and low temperature, has greatly simplified the setup and presented a novel synthesis route for DLC films and carbon films. The low potential made it feasible to control the deposition process simply by charge. Meanwhile, the low temperature (less than –40 ^{o}C) made this method suitable for any substrate, which is unstable at high temperature. However, V. P. Novikov and V. P. Dymont et al.'s reports [28-31] left many things unexplored such as its application to different substrates, the effects of different parameters on the deposition of DLC films and the potential to deposit other thin films. It is both necessary and rewarding to explore this method in more details. In this chapter, employing the above method, various substrates were tried with a three-electrode system. Temperature, potential, current, the distance between working electrode and counter electrode as well as other parameters were changed to measure their effects on the deposition of DLC films.

2.2. Experimental

A variety of substrates including Ni, Cu, Co, Mo, Brass, Iron and stainless steel were used in this study. All of them were more than 99.99% pure. They were cut into a 10 × 10 × 0.25 mm^3 size and connected to a copper wire using conductive silver epoxy, then mounted by epoxy to prevent the copper wire from coming into direct contact with the electrolyte. Traditional mechanical polishing method was used to obtain a mirror finish on the substrates. The abrasives, laps and lubricants used in every polishing step are shown in Table 2.1.

Table 2.1. Polishing steps of Ni substrates

Step	Abrasive & Size	Lap or Wheel Covering	Lubricant
1	SiC 320 grit	Disc	Water
2	SiC 400 grit	Disc	Water
3	SiC 600 grit	Disc	Water
4	Diamond Paste (6 μm)	Nylon Cloth	Diamond extender
5	Diamond Paste (1 μm)	Nylon cloth	Diamond extender
6	Gamma Alumina (0.05 μm)	Lecloth	Alumina solution in water

Mirror finish substrates were finally ultrasonically cleaned in de-ionized water for 20 min and wiped using a tissue before deposition. The whole process can be illustrated by

Figure 2.1. An electrochemical cell consisting of three electrodes was used in this study as shown in Figure 2.2.

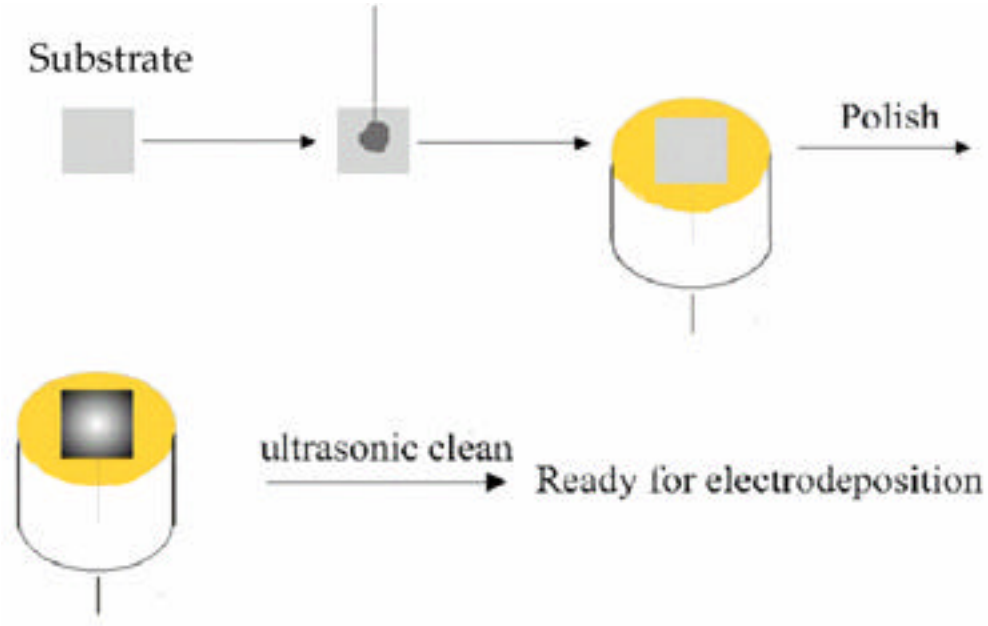

Figure 2.1. Substrate preparation process

Before the experiment, three electrodes were first placed in the vessel. The polished substrate was connected as the working electrode (WE), Pt foil with a size of 10 × 10 × 0.25 mm^3 connected to a copper wire as counter electrode (CE) and Pt wire as pseudo reference

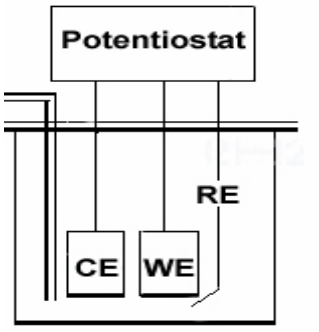

Figure 2.2. Electrochemical cell setup

electrode (RE). The working electrode was placed parallel to the counter electrode and the tip of the reference electrode was placed as close as possible to the working electrode. Using this arrangement, the current was passed between the working electrode and counter electrode and the potential of working electrode was monitored relative to the reference electrode. Then the air was pumped out of the vessel through a simple vacuum pump for 10 minutes to expel the air and avoid water and CO_2 condensation. Ammonia gas, anhydrous grade, was bubbled into the vessel and liquefied until the solution completely covered the substrate. The liquefication was accomplished by immersing the vessel in a cold acetone/dry ice bath. Finally, acetylene was fed into the vessel continuously and saturated in the liquid ammonia electrolyte during the whole electrodeposition process. An EG&G Model 263 A Potentiostat/Galvanostat was connected to the three electrodes as the voltage supply. The experiments were operated with galvanostatic method and potentiostatic method respectively. The electrodeposition was carried out at a voltage in the range of 1.4 - 6.0 V. The current density and the temperature were in the range of -2.2 to - 0.10 mA/cm^2 and -72 to -40 ^{o}C respectively.

After electrodeposition, the substrate was taken out of the vessel and washed with deionized water. The morphology of DLC films was imaged using a JSM-T 300 scanning electron microscopy (SEM) with accelerating voltage 20 KV. Raman analysis was performed with either an Almega Dispersive Raman microscopy consisting of an extended range TE Cooled Charge Coupled Detector (CCD) using 532 nm laser excitation or a Jobin Yvon T64000 system using 632.81 nm He-Ne laser excitation. The elemental composition was analyzed using X-ray photoelectron spectroscopy (XPS). XPS

is carried out on a VG Escalab MK II system by twin anode (Al Ka X-ray source) with a 20 eV pass energy and calibrated by assigning the energy of the C1s peak due to carbon contamination (referred to as adventitious carbon) on the sample to the accepted value of 284.6 eV. Fourier transform infrared (FTIR) absorption spectroscopy was used to identify the characteristic bonding of the films.

2.3. Results and Discussion

Ni, Cu, Co, Mo, Brass, Iron and stainless steel substrates were all tried using the same method with conditions slightly changed. Different substrates have shown different results. First, let us concentrate on the results of Ni substrates.

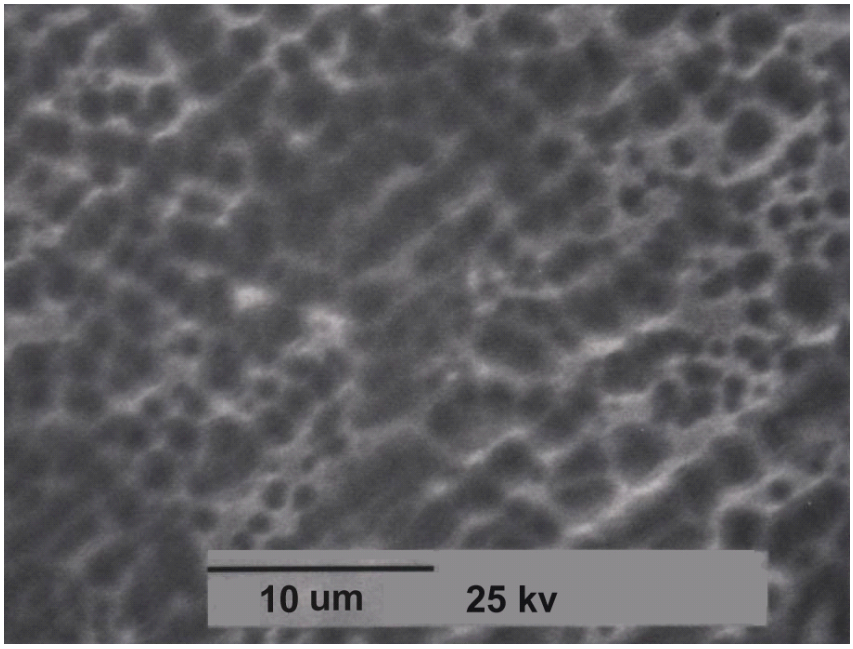

Figure 2.3. SEM image of films on Ni sample 1

2.3.1. Scanning Electron Microscopy (SEM)

Scanning electron microscopy was used to image deposits on every Ni sample. Although the appearance of deposits varied, the most common morphology is shown in Figure 2.3. It can be seen that there are some continuous pits with an average size of approximately 1 ?m in the film.

2.3.2. Raman Spectroscopy

Raman spectroscopy of as-deposited film on a Ni sample is shown in Figure 2.4. The shoulder D peak at 1365 cm^{-1} and broad G peak at 1558 cm^{-1} were indicative of a DLC film. The G peak at 1558 cm^{-1} was attributed to the graphite-like layers of sp^2 micro

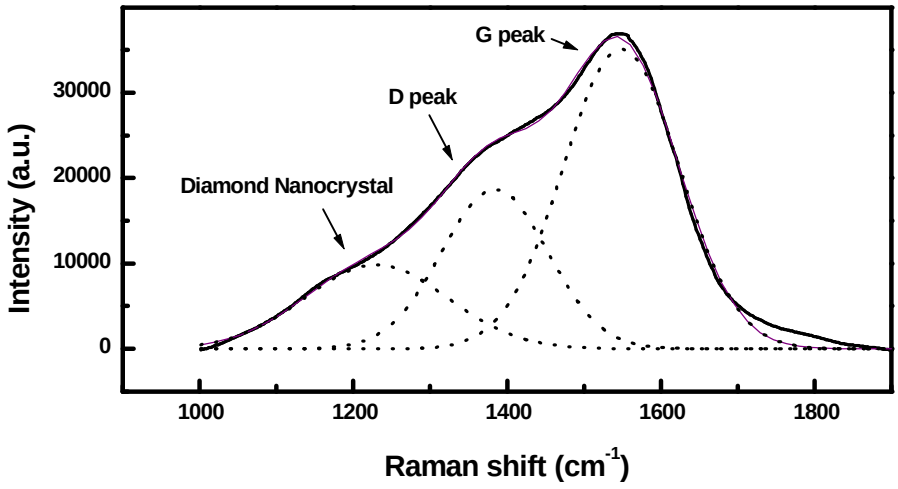

Figure 2.4. Raman spectra of the films on Ni sample 1

domains, while the D peak at 1365 cm^{-1} corresponded to the bond-angle disorder in the sp^2 graphite-like micro domains induced by the linking with sp^3-C atoms as well as the finite crystalline sizes of sp^2 micro domains [35-37]. To quantitatively measure the intensity ratio of D peak to G peak, the Raman pattern was further deconvoluted through a gaussian curve-fitting procedure through software origin 5.0. Three peaks were shown in the spectra after deconvolution. From the dashed separate peaks shown in Figure 2.4, it was found that the intensity ratio of D peak to G peak (I_D/I_G) was nearly 0.54. Besides these two peaks, a shoulder peak at around 1230 $cm^{-1}$is also shown in the gaussian-fitting curves. It was assigned to diamond nanocrystals according to Gonon et al. (40) and Popovici et al. (41). This reveals that some diamond nanocrystals are also deposited during the time of the formation of DLC films.

2.3.3. X-ray Photoelectron Spectroscopy

XPS spectrum of the DLC film on a Ni sample is shown in Figure 2.5. The sharp C1s peak with binding energy 286.3 eV indicated that the main constituent of the DLC film was carbon. Through gaussian curve-fitting procedure, the C1s peak can be deconvoluted into two peaks. One of the peak occurs at 285.6 eV, which is due to sp^2 carbon, and the other one occurs at 287.3 eV, which is due to sp^3 carbon. According to some other reports [49-52], the C1s peak is at 284.3 eV in graphite and 285.75 eV in diamond. The higher shift of C1s in this study are still under investigation. Except for the C1s peak, a strong O1s peak is also shown in XPS spectrum. Due to insensitivity of XPS to H atom, the existence of H atom cannot be concluded here.

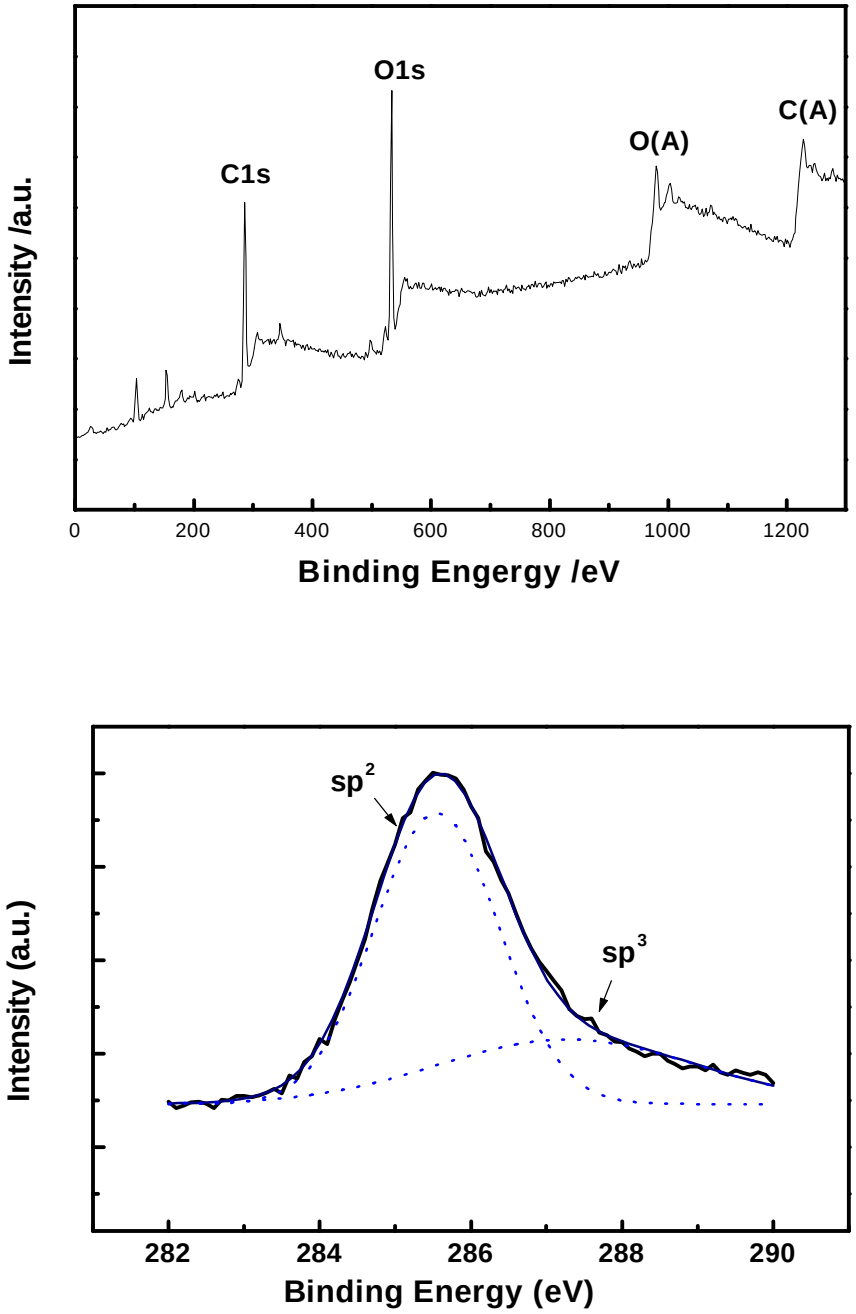

Figure 2.5. XPS of the films on Ni sample 1: (a) Overview of XPS spectrum. (b) C1s,

XPS

2.3.4. Fourier Transform Infrared Spectroscopy

FTIR absorption spectra of deposits on Ni is shown in Figure 2.6. It features three peaks in the region 2840-2975 cm^{-1} characteristic of C-H stretching vibrations. The peaks at 2955, 2925 and 2854 cm^{-1} correspond to the sp^3 CH_3 asymmetric, sp^3 CH_2 asymmetric and symmetric stretching vibrations respectively [44]. This showed that hydrogenated diamond-like carbon films were deposited in our study and hydrogen is preferably bonded to sp^3 carbon.

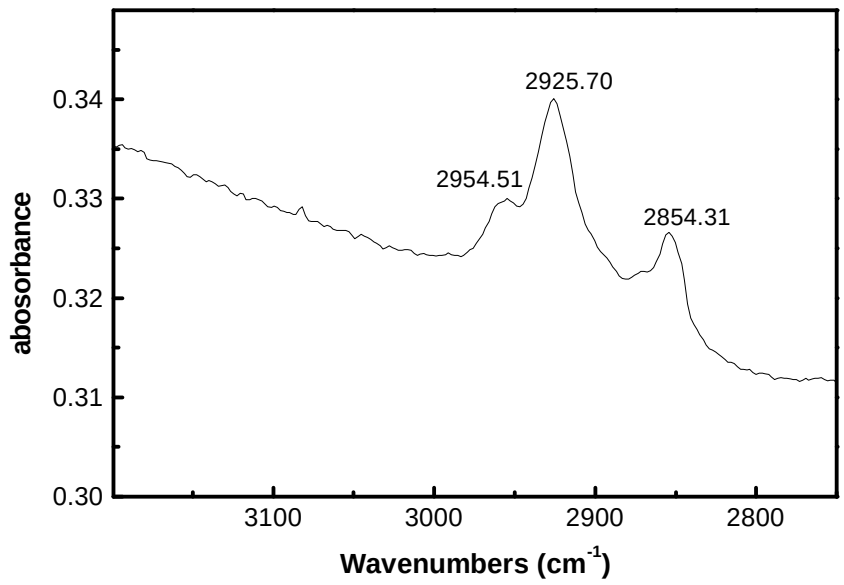

Figure 2.6. FTIR spectra of the films on Ni sample 1

2.3.5. Electrical Resistance

By recording the potential and current during this study, it was found that the electrical resistance R, composed of a series of resistances involved in the electrode reaction,

increased as the reaction proceeded. Figure 2.7 is the time-dependence curve of R in Ni sample 1. It shows that the electrical resistance increases as the reaction moves on until it finally reaches a maximum value. This may be mainly due to the surface change of the Ni substrate. The insulating DLC film deposited gradually covers the Ni surface, directly resulting in the increase of the resistance. After a compact DLC film completely covers the surface, the resistance will reach a maximum value and remain unchanged.

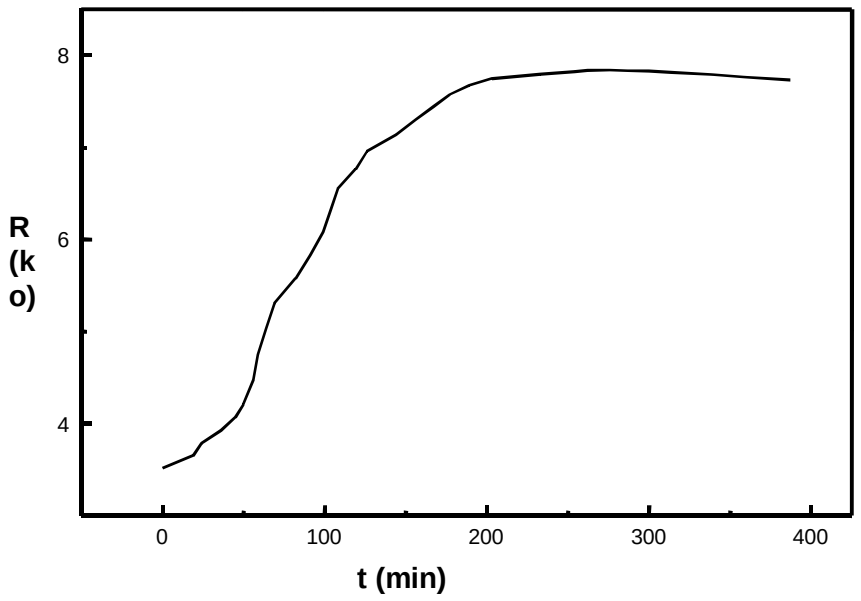

Figure 2.7. Time dependence curve of the electrical resistance

2.3.6. Effects of Experimental Parameters

Several identical Ni substrates have been tried with different conditions to study the effects of experimental parameters on the deposition of DLC films. The experimental parameters for each sample are listed in Table 2.2. It is noticed that, in this study, all

parameters for these samples are randomly changed, therefore an exactly individual effect of every parameter on the nucleation and formation of DLC films is hard to obtain.

Table 2.2. Experimental conditions for Ni samples

No	Method	WE	CE	E(V)	I(mA)	Q(C)	T(^{o}C)	Time	Color
1	Galvanostat	Ni	Pt	4.50-1.70	-1.00 ~ -0.35	-10.7	-55 ~ -50	6.5 h	Brown
2	Galvanostat	Ni	Pt	5.00-1.40	-2.00 ~-0.30	-8.17	-70 ~ -65	2.8 h	Gray
3	Potentiostat	Ni	Pt	4.00-1.40	-0.66 ~ -0.03	-3.52	-72 ~ -66	5.2 h	Gray
4	Potentiostat	Ni	Pt	6.00-2.20	-2.20 ~ -0.10	-8.7	-65 ~ -40	4.4 h	Brown

A number of factors may affect the deposition of DLC films, including I_D/I_G, thickness of DLC films, morphology, hardness, elastic modulus as well as the position of D peak and G peak. To study the individual effect of every parameter on the deposition of DLC films, it is desirable to design a series of experiments, in which only one parameter is systematically changed while keeping all of the other parameters constant, and then compare the DLC films in terms of the aspects mentioned above.

Although very limited, some important information can still be obtained based on the results. From the spectra as shown in Figure 2.4 and Figure 2.8, the D peak and G peak occur at the same position for all four Ni samples. Since the overall effect of all parameters on the position of D peak and G peak in the Raman spectra is negligible, it can be concluded that none of the parameters has any obvious effect on the position of D peak and G peak either. Otherwise, any such obvious effect will surely result in an overall significant effect. In this study, sample 1 and 2 were electrodeposited in

galvanostat method, and sample 3 and 4 in potentiostat method. Galvanostat and potentiostat are two different electrochemical methods. In galvanostat, the current was controlled, while the potential difference was determined as a function of time. On the contrary, in potentiostat, the potential difference between the working and reference electrodes was controlled, while the current was determined as a function of time. As shown in Figure 2.4 and Figure 2.8, these two methods had no significant influence on the Raman spectra of DLC films. It is in agreement with the fact that the difference between these two methods mainly shows itself in the study involving surface boundary condition, double-layer charging effects and background process [53], which have limited effect in this study.

To prevent the EG&G Model 263 A Potentiostat/Galvanostat instrument from overloading, the current was manually decreased in the galvanostat method and the potential was decreased in the potentiostat during the electrodeposition process. It was believed that current, potential as well as deposition temperature, charge consumed and distance between WE and CE all have important influence on the deposition of DLC films. Due to the random change of the parameters, no conclusion can be made based on this study.

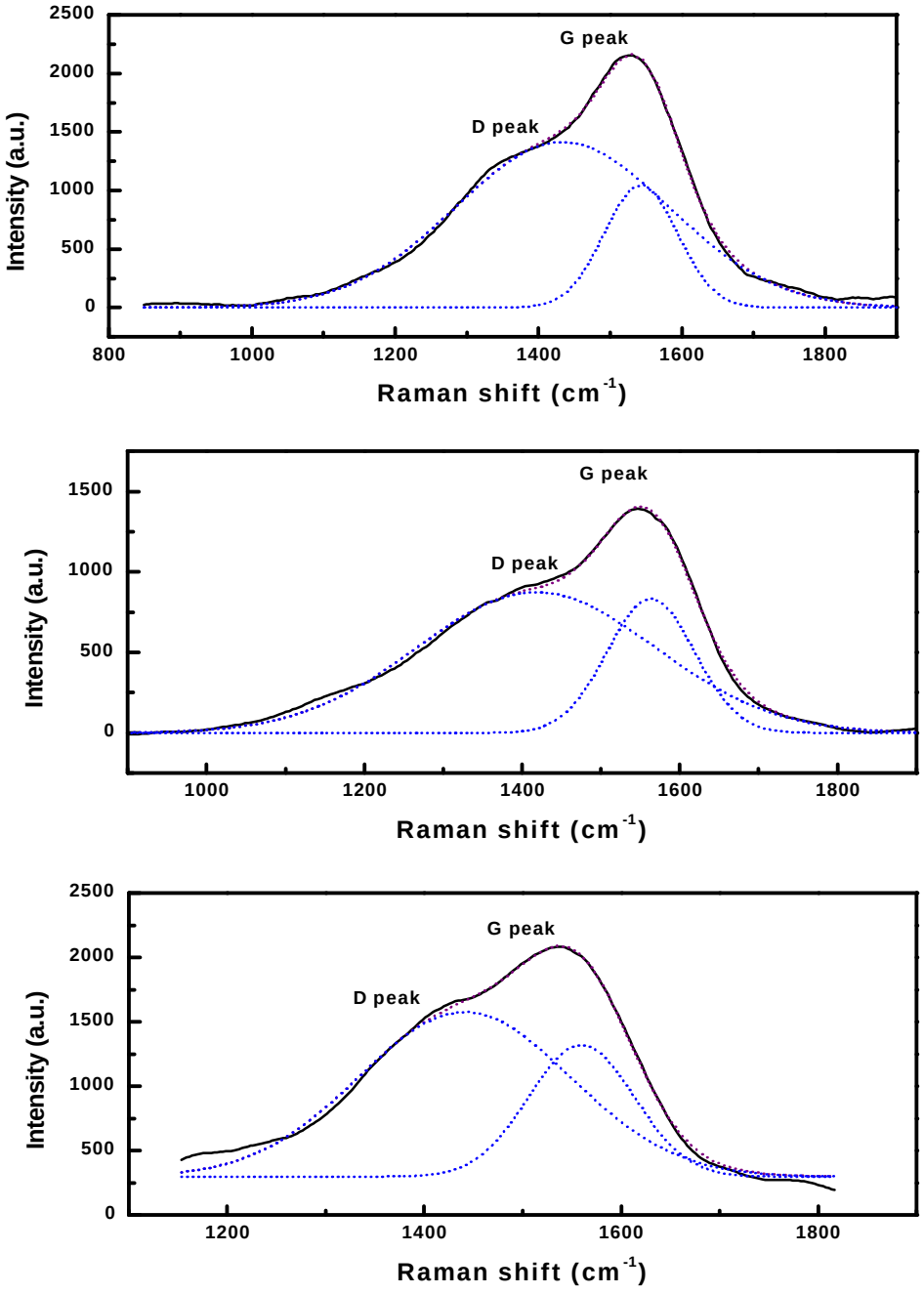

Figure 2.8. Raman spectra of the films on Ni (a) sample 2 (b) sample 3 (c) sample 4

2.3.7. Effects of Substrates

Ni, Cu, Brass, Co, Mo, Iron and stainless steel were used as substrates in this study. Raman spectra showed that DLC films were successfully deposited on Ni, Cu, and Brass substrates by this method. But no DLC films were deposited on Mo, Co, Iron and stainless steel substrates.

The Raman spectra for Ni, Cu and Brass samples are shown in Figure 2.4, 2.9 and 2.10. They are similar in that the D peak occurs at around 1358 cm^{-1} and the G peak at around 1580 cm^{-1} for all spectra. However, there are many differences among them. First, the I_D/I_G of Ni samples is much lower than that of Cu and Brass samples. According to Tuinstra et al. [35], I_D/I_G is inversely proportional to the sp^3/sp^2. The lower I_D/I_G of Ni samples demonstrated that the ratio of sp^3 to sp^2 carbon in Ni sample is higher than that of Cu and Brass samples. Second, the three substrates demonstrated different properties for the formation of diamond nanocrystal. As discussed earlier, diamond nanocrystal was formed on some Ni samples. From Figure 2.9 and 2.10, it was found that the diamond nanocrystal was also formed on Cu sample but not on Brass sample. The real mechanism for the formation of diamond nanocrystal is still under investigation. However, it was believed that some nucleation sites on the Cu substrate as well as Ni substrate helped the formation of diamond nanocrystals. In addition, from the Raman spectra, it was further found that the intensity of nanocrystal peak for Cu sample is much stronger than that for Ni samples.

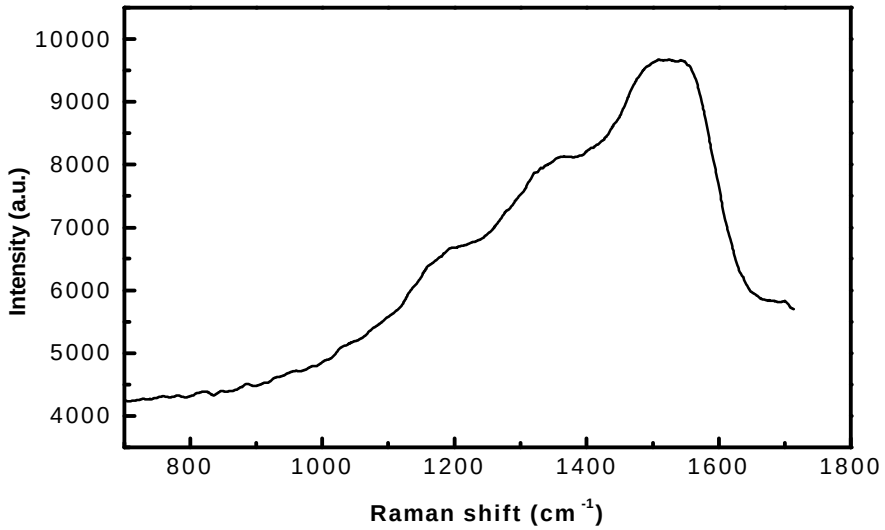

Figure 2.9. Raman spectra of films on Cu sample

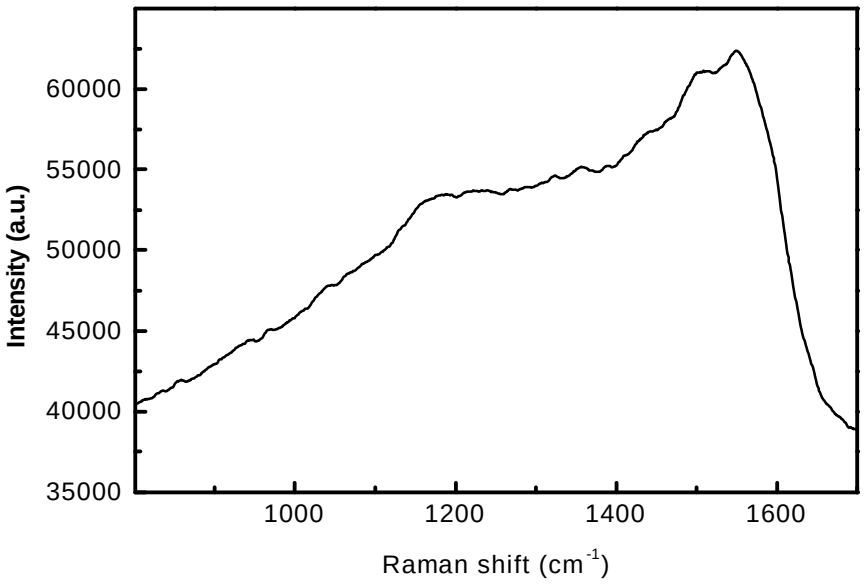

Figure 2.10. Raman spectra of films on Brass sample

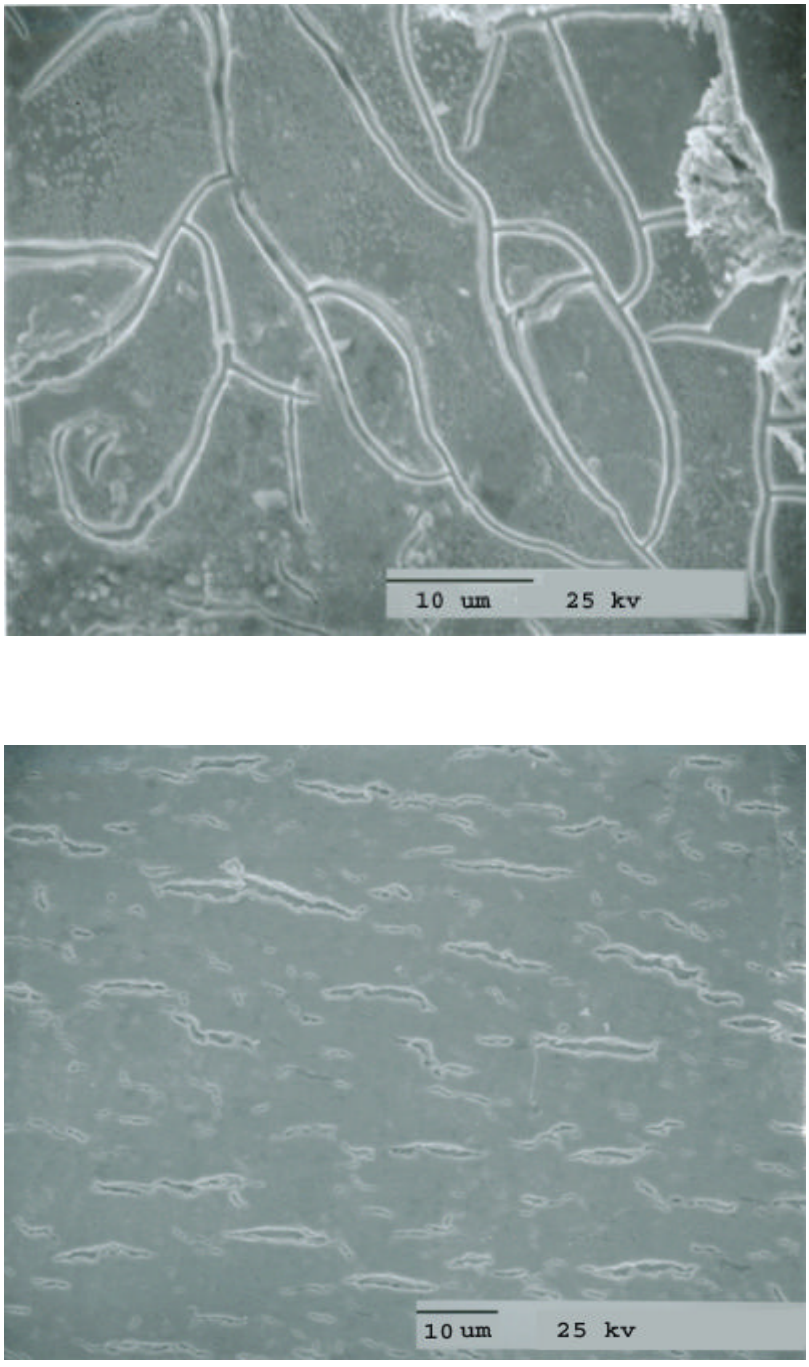

Figure 2.11. SEM image of films on Cu sample at two different parts

SEM images of Ni samples and Cu samples are shown in Figure 2.3 and Figure 2.11 respectively. From the image of Ni samples, it can be seen that some continuous pits with an average size of approximately 1 ?m occur in the film. From the image of Cu samples, it was found that there are some cracks in the film and some small nucleation sites were evenly spread on the surface of the films. The existence of the nucleation sites on top of the thin films indicates that the electrodeposition process can be governed by a progressive nucleation growth. Continuation of deposition is achieved through the formation of new nuclei on the existing deposit. Also the cracks indicate some crystallites were formed during the elctrodeposition process. These SEM results have partially explained the formation of diamond nanocrystals and the higher intensity of diamond nanocrystal Raman peak on the Cu sample.

2.3.8. Cyclic Voltammetry (CV)

To study the electrodeposition mechanism, cyclic voltammetry is run in this study. A liquid ammonia solvent system before addition of C_2H_2 and a saturated solution of C_2H_2 in liquid ammonia were both scanned between 2 V and 6 V at a scan rate of 40 mV/s and a temperature of -40 ?C. The results are shown in Figure 2.12. As shown in Figure 2.12, it is found that no typical cyclic voltammogram was observed for either solution. On the contrary, two straight lines which show a linear relationship between potential and current are observed. Assuming the overall conductance of the electrochemical circuit can be ascribed to the solvent system or the solution system, the conductance of liquid

ammonia before addition of C_2H_2 and saturated solution of C_2H_2 in liquid ammonia can be respectively calculated from the following equation:

$$G ? \frac{I}{E} \quad (2.1)$$

where G is the conductance, I is current density and E is the voltage.

From the calculation, the conductance of liquid ammonia was found to be 7.3 ? 10^{-5} ? $^{-1}$ and that of saturated solution of C_2H_2 in liquid ammonia was 4.9 ? 10^{-5} ? $^{-1}$. According to Chapter 1, systems with such low conductance are not suitable for an effective CV study. To increase the conductance, a small amount of sodium acetylide was added into the liquid ammonia solvent as supporting electrolyte. Then the solution system before addition of C_2H_2 and saturated solution of C_2H_2 in liquid ammonia with sodium acetylide as supporting electrolyte were respectively scanned again at the same scan rate. Two similar straight lines were still observed for both solutions. Using equation 2.1, the conductance was found to be 1.1 ? 10^{-4} ? $^{-1}$ and 1.7 ? 10^{-4} ? $^{-1}$ respectively. Although the conductance was obviously increased, it is still too low to conduct an effective CV study.

Through our study, it was impossible to conduct a CV study on our solvent and solution system due to the low conductance. But the straight line obtained from the CV scan provided an approximate method to calculate the conductance of the electrochemical system. Based on the value of conductance, some important information could be obtained. First, the liquid ammonia solvent system in this study has a conductance of 7.3 ? 10^{-5} ? $^{-1}$. As far as the electrochemical system in this study is concerned, it is reasonable to imagine the electrochemical cell as a conductor.

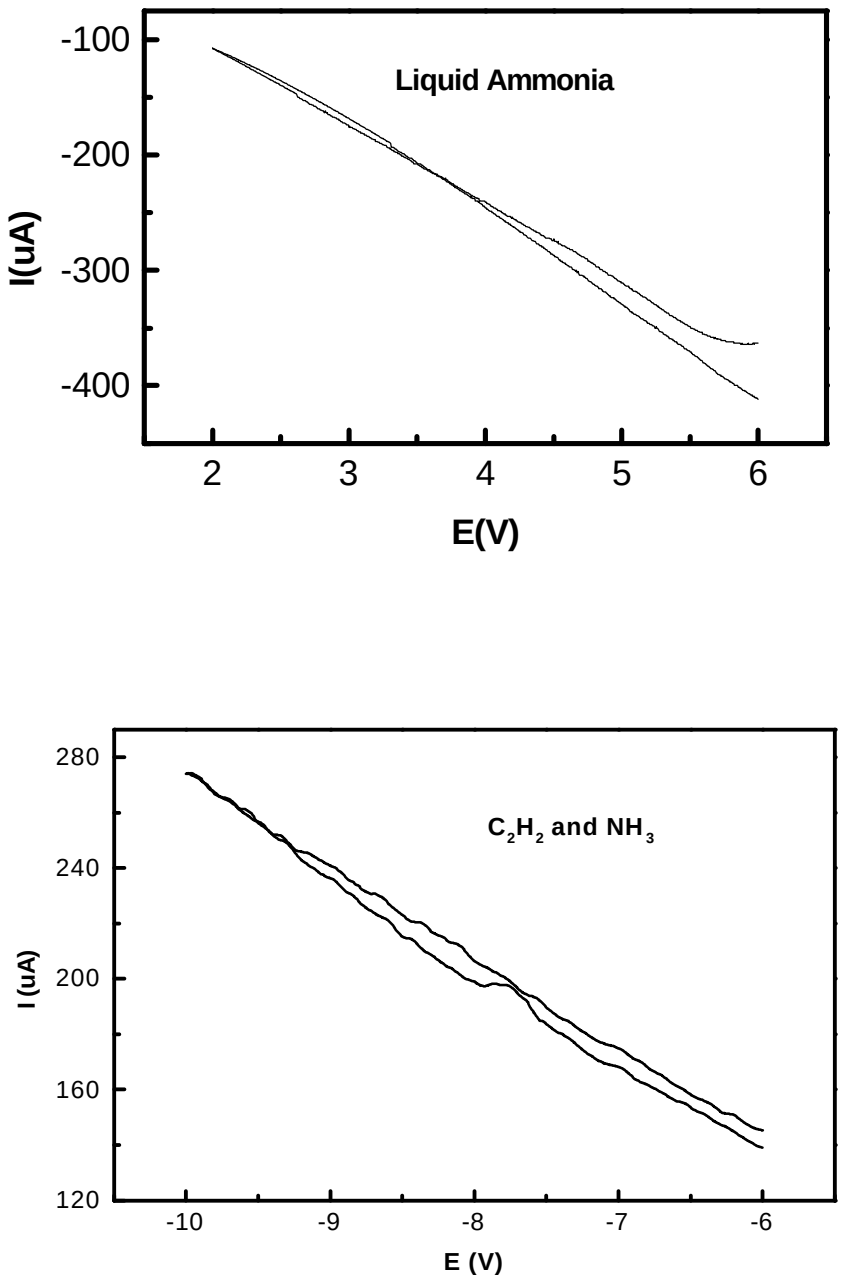

Figure 2.12. CV result of pure liquid ammonia and saturated solution of C_2H_2 in liquid ammonia

Then the length of the conductor can be imagined as the distance between WE and CE, that is 1 cm, and the cross-sectional area imagined as the area of the substrates, that is 1 cm^2. According to the following equation:

$$? ? G\frac{l}{A}, [?] ? Sm^{?1}, Scm^{?1} \qquad (2.2)$$

where G is the conductance, l is the length of conductor, A is the cross-sectional area of conductor and ? is the specific conductance.

The specific conductance of the liquid ammonia system is calculated to be 7.3 ? 10^{-5} ? $^{-1}cm^{-1}$. Compared to the ordinary conductance order of a pure liquid ammonia system, that is 10^{-7} ? $^{-1}cm^{-1}$, the specific conductance of our liquid ammonia system is nearly three orders higher. The increase of conductance has shown that some sources of contamination, such as the residual vapor, have been introduced into the liquid ammonia system in this study. Second, it was found that the conductance of the liquid ammonia system with a small amount of sodium acetylide was far below its limiting equivalent conductance 262 ? $^{-1}cm^2$ as discussed in Chapeter 1. This inconsistency is still under investigation.

In addition, KI was also tried in this study as supporting electrolyte to increase the conductance. Although it could effectively increase the conductance, its decomposition under the positive potential scanned made it unsuitable for this study.

2.3.9. Mechanism of Electrodeposition of DLC films

As reported by V.P.Novikov et al. [28-30], the electrodeposition of DLC films with this method may be separated into two steps, that is the electrolytic dissociation of acetylene to H^+ and C_2H^- and the oxidation of anion ion C_2H^- to C_{2n} or $C_{2n}H_n$ at the anode. However this mechanism is susceptible given the high binding energy of C-H bond in HC?CH. It is very difficult to dissociate C_2H_2 to H^+ and C_2H^- at such a low electric field. Liquid ammonia is an amphiprotic, very weakly acidic, slightly ionized solvent in which solvated electrons are stable [42]. So it is possible that the first step is the formation of solvated electrons followed by the reversible reduction of C_2H_2 to produce anion radicals.

$$C_2H_2 + e^-_{solv} \; ? \quad C_2H_2? \qquad (2.3)$$

Then anion radicals $C_2H_2?$ moves into the anode area and is further oxidized to carbon films by the anode. More work needs to be done to explore the real mechanism.

Overall, a tremendous advantage that electrodeposition gives over the other deposition techniques is that the nucleation and growth can be studied in-situ while the deposition is occurring. As for an electrode reaction, the following relations are well known [53],

$$i\,(\text{amperes}) \; ? \; \frac{dQ}{dt}\,(\text{coulombs/s}) \qquad (2.4)$$

$$\frac{Q\,(\text{coulombs})}{nF\,(\text{coulomb/mol})} \; ? \; N\,(\text{mol electrolyzed}) \qquad (2.5)$$

where a direct proportionality between the coulombs of electric charge flowing through the electrode and the moles of reactant electrolyzed is demonstrated. Furthermore, for such a heterogeneous electrode reaction as involved in our study, occurring only at the

electrode-electrolyte interface, the reaction rates can be described by the following equation:

$$\text{Rate}\,(\text{mols}^{?1}\text{cm}^{?2}) \;?\; \frac{i}{nFA} \;?\; \frac{j}{nF} \quad (2.6)$$

It shows that the actual deposition growth rate is directly determined by the current during electrodeposition, and the mass or the thickness of deposited DLC films can even be measured directly from the charge going through the electrode assuming the current efficiency of current is known.

2.4. Conclusion

Through this study, the electrochemical method using a three-electrode cell has proven effective to deposit typical DLC films on Ni, Cu and Brass substrates at low potential and low temperature. SEM, Raman, FTIR and XPS were successfully employed to characterize the properties of as-deposited DLC films.

To study this method in more details, much more research needs to done. This includes, but not limited to the following aspects: individual effect of every parameters on the deposition of DLC films, the nucleation growth of diamond nanocrystals and the cyclic voltammetry study of electrodeposition of DLC films with the aid of a suitable supporting electrolyte.

References

49. A. E. Henderson, A. G. Fitzgeralt, D. S. Rickerby and B. E. Storey, Electron Spectroscopy and Electron Microscopy of a-C:H Films, Journal of Electron Spectroscopy and Related Phenomena, 52 (**1990**) 475.

50.V. N. Apakina, A. L.Karuzskii, M. S. Kogan, A. V. Kvit, N. N. Melnik, Y. A. Mityagin, V. N. Murzin, A. A. Orlikovsky, A.V. Perestoronin, s. D. Tkachenko and N. A. Volchkov, Diamond and Related Materials, 6 (**1997**) 564.

51. P. Merel, M. Tabbal, M. Chaker, S. Moisa and J. Margot, Direct Evaluation of the sp3 Content in Diamond-like-carbon Films by XPS, Applied Surface Science, 136 (**1998**) 105.

52. I. A. Akwani, E. D. Sosa, S. C. Lim, R.E. Stallcup II, J. N. Castillega, J. Bernhard, D. E. Golden and J. M. Perez, Effect of $sp^3/(sp^2 + sp^3)$ Carbon Fraction on the Photoelectric Threshold and Electron Affinity of Diamond Films, Mat. Res. Soc. Symp. Proc, 509 (**1998**) 137.

53. Allen J. Bard, Larry R. Faulkner, Electrochemical Methods, 2^{nd} edition. 21 (**2001**)

CHAPTER 3

ELECTRODEPOSITION OF DLC FILMS USING TWO-ELECTRODE SYSTEM

3.1. Introduction

In chapter 2, a three-electrode system was used to successfully deposit DLC films on Ni, Cu and Brass substrates. The use of a pseudo reference electrode helped the stabilization of the electrochemical reaction in non-aqueous solution [53]; Second, the working electrode was connected as positive electrode. Therefore, as discussed in section 2.3.9, the deposition of DLC films on working electrode was ascribed to the oxidation of C_2H_2 at the working electrode. Cyclic voltammetry was tried to confirm the oxidation reaction mechanism. However, due to the low conductivity of electrolyte, no typical cyclic voltammogram was observed. The real deposition mechanism is still unknown.

In addition, as previously discussed, much research has been done to deposit DLC films directly from organic liquids at high potential [14-26]. In their research, a working electrode was connected as the negative electrode with DC power as electricity source. The organic liquids used consisted of two parts, the alkyl group (A=CH_3, or C_2H_5) and a large electrophilicity group (X=CN, NHCOH, and OH). It was proposed that when a high voltage was applied to the electrode, these molecules were polarized; two groups became partly discharged groups and moved in the electric field. The CH_3 or C_2H_5 groups with a part of the positive charge would adsorb on the surface of the cathode and then be deposited as DLC films. In this research, a high electric field has to be applied to

dissociate the covalent bonds between the CH_3 or C_2H_5 groups and X groups. The applied voltages were generally more than 1000 V.

The above electrophoresis mechanism as well as the oxidation mechanism in our study both successfully explained the deposition of DLC films using the corresponding methods. However, none of the mechanisms was tested by effective analysis methods. What's more, as discussed in Chapter 1, although the electrodeposition of DLC films directly from organic liquids using high potential was proved very successfully, the high potential has greatly increased the difficulty to control the deposition process and complicated the setup.

Motivated by the interests to probe the mechanism of electrodeposition of DLC films and conquer the disadvantages of the electrodeposition using high potential, a new electrodeposition method was developed for the first time, which is discussed in this chapter.

In this method, most experimental conditions were the same as used in Chapter 2. A solution of C_2H_2 in liquid ammonia was also used as the carbon source. However, instead of being connected as positive electrode, the working electrode was connected as negative electrode, which made the oxidation mechanism unsuitable. At the same time, a potential as low as 30 V was applied to the two electrodes through a DC power, which made the mechanism based on a high electric field unsuitable.

3.2. Experimental

Four substrates Ni, Mo, Brass and stainless steel were all tried in this study. The schematic diagram of the deposition system of this investigation is shown in Figure 3.1.

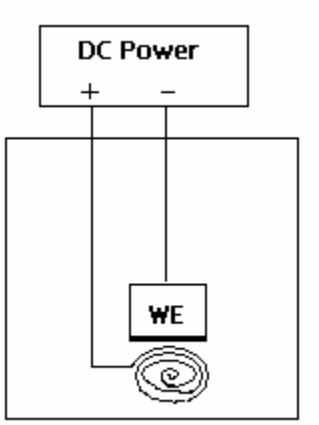

Figure 3.1. Schematic illustration of electrochemical cell setup

A negative potential –30 V was applied to the working electrode through a DC power. A Ni-Cr wire was twisted into circles as the counter electrode as shown in Figure 3.1. The distance between working electrode and counter electrode was kept in the range of 3 mm to 8 mm. The current density and the temperature were in the range of 2.30 to 0.10 mA/cm^2 and –70 to –45 ?C respectively. Experimental procedures generally followed those described in Chapter 2.

The deposits were characterized by Raman spectroscopy using 632.85 nm laser excitation and Fourier Transform Infrared Spectroscopy (FTIR).

3.3. Results and Discussion

Raman spectra showed that typical DLC film was only successfully deposited on Ni substrates. The Raman spectra of deposits on Ni sample 5 is shown in Figure 3.2.

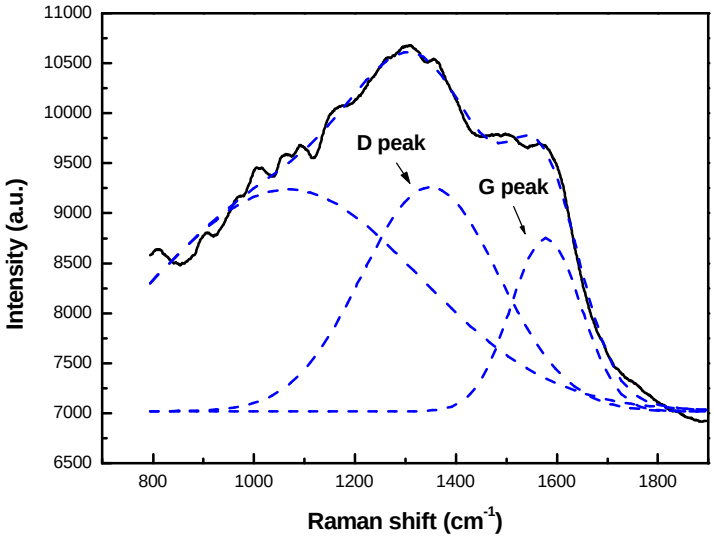

Figure 3.2. Raman spectra of the films on Ni sample 5

By the same gaussian curve-fitting procedure as used in Chapter 2, the peak was deconvoluted into three peaks. Two peaks characteristic of DLC films, D peak and G peak, occured at 1349 cm^{-1} and 1578 cm^{-1} respectively, which is similar with the results previously discussed in Chapter 2. A third peak was positioned at 1067 cm^{-1}. Compared with the diamond nanocrystal peak of Raman spectra as shown in Figure 2.4, this peak has a lower shift of about 160 cm^{-1}. However, given the similarity of these two methods, it is reasonable to assign this peak to the diamond nanocrystal. The fraction of diamond nanocrystal peak, D peak and G peak by area was calculated to be 0.58 : 0.30 : 0.12. This

result is interesting especially in terms of two aspects. First, it showed that the new electrochemical method is more beneficial to the formation of diamond nanocrystals according to its high fraction in Raman spectra. This partially demonstrated the possibility to deposit diamond crystals using this method. Second, the high ratio of D peak to G peak showed a low fraction of sp^3 carbon in the DLC films [35]. From this result, it can be assumed that the sp^3 carbon, once formed, is probably transformed into diamond nanocrystals through some certain mechanism.

FTIR absorption spectra of deposits on Ni substrates has shown no peaks in the region 2840-2975 cm^{-1}, which is characteristic of C-H stretching vibrations. From this result, it can be concluded that, compared with the DLC films produced by the previous method as discussed in Chapter 2, less hydrogenated or hydrogen free DLC films were deposited on Ni substrates by this new electrochemical method.

Oxidation mechanism successfully explained the deposition of DLC films by the previous method in Chapter 2. It is noticed that, in that method, the working electrode was connected as positive electrode. If this mechanism also controlled the deposition process in this new electrochemical method, it can be imagined that DLC films should be deposited on the positive counter electrode, which, however, does not occur.

On the other hand, it is also unsatisfactory to explain the deposition process using the electrophoresis mechanism. Based on the electrophoresis mechanism, C_2H_2 has to be dissociated into a carbon-containing cation ion. This is difficult for this new electrochemical method. First, the electric field with a 30 V potential difference between

counter electrode and working electrode is not strong enough to dissociate the C_2H_2. Second even if dissociated, C_2H_2 is more likely to be dissociated into H^+ and C_2H^-.

From the above discussion, it was believed that some other deposition mechanisms were responsible for the deposition of DLC films by the new electrochemical method. In addition, it is to be especially realized that the three-electrode system and two-electrode system have demonstrated some different effects on the deposition process, which, has not been well investigated up to now.

3.4. Conclusion

The new electrochemical method developed in this study has successfully deposited typical DLC films and diamond nanocrystals on Ni substrates. The films were respectively characterized by Raman spectroscopy and FTIR. Raman spectra showed a high fraction of diamond nanocrystals in the films. FTIR results showed the DLC films were less hydrogenated or hydrogen free compared with the previous results in Chapter 2.

The success of this new method to deposit DLC films as well as diamond nanocrystals has greatly broadened the application of electrochemical methods into the deposition of carbon films.

CHAPTER 4

CONCLUSION

Two electrochemical methods have been successfully used to deposit diamond-like carbon (DLC) films on a variety of substrates from the solution of acetylene in liquid ammonia.

The first electrochemical method was first developed by V. P. Novikov et al. [28] in 1996. My study has mainly emphasized on the development of this method and its application on different substrates. A three-electrode system, which consists of working electrode, counter electrode and reference electrode was used to carry out the electrodeposition process. A low potential (<10V) was positively applied into the working electrode and the current density was in the range of -2.2 to -0.10 mA/cm^2. A series of results have shown that through this method, typical hydrogenated DLC films can be deposited on Ni, Cu and Brass substrates but not on Co, Mo, Iron and stainless steel substrates. SEM, Raman spectroscopy, FTIR and XPS were all used to characterize the as-deposited films. From Raman spectra and SEM, diamond nanocrystals were further found to form on Ni and Cu samples. Given the specific properties of this method and the electrochemical cell setup, an oxidation mechanism was postulated to control the electrodeposition process.

Based on the above electrochemical method, a new electrochemical method was developed by my own for the first time to deposit DLC films on Ni substrates. This method used a two-electrode system consisting of working electrode and counter electrode. A negative potential (-30 V) was applied into the working electrode. Initial

results have shown that through this method, hydrogen free DLC films were successfully deposited on Ni substrates but not on brass, Mo and stainless steel substrates. The as-deposited films were characterized by Raman spectroscopy and FTIR. According to the Raman spectra, it was found a much higher fraction of diamond nanocrystals were formed on the Ni substrates compared with the results using the first method. It was believed neither oxidation mechanism nor the electrophoresis mechanism controlled the deposition process in this new method. However, the real mechanism is still unknown.

The success of electrochemical methods to deposit DLC films and diamond nanocrystals is very promising. It has initiated me for future work, one of which is the possibility to deposit boron-doped diamond films through electrochemical methods.

Boron-doped diamond films have been widely studied due to its excellent electrochemical properties [54-64]. Boron-doped diamond electrodes has a large potential window, extreme chemical stability, low voltammetric background currents, low double layer capacitance and high resistance to deactivation. Hot-filament chemical vapor deposition (HFCVD) and microwave plasma-assisted chemical vapor deposition (MPCVD) were the commonest methods to produce boron-doped diamond films. In these methods, boron source mainly include B_2H_6, B_2O_3-CH_3OH/$(CH_3O)_3B$, $B(CH_3)_3$, BF_3 or 2-alkyl-1,2-oxaborolane, most of which are dangerous or explosive. However, through an electrochemical method, the low temperature and low potential will make these boron sources safer. What's more, organic compounds which include both carbon atom and boron atom will be ideal boron sources for electrochemical methods. My proposed electrodeposition of boron-doped diamond films is based on a combined mechanism of

oxidation/reduction mechanism and electrophoresis mechanism and an organic compound containing both carbon and boron atom is used as the carbon and boron source. It is also supposed this organic compound should be dissociated into cation and anion ion under a certain electric field. The method is slightly altered depending on the properties of the organic compound. After dissociation, if the carbon and boron atom are both included in the cation ion, a negative potential will be applied into the working electrode. Due to the electrophoresis mechanism, the cation ions will move into the working electrode area and boron-doped diamond films can be deposited on the substrates by reduction. On the contrary, if the carbon and boron atom are both included in the anion ion after dissociation, a positive potential will be applied into the working electrode.

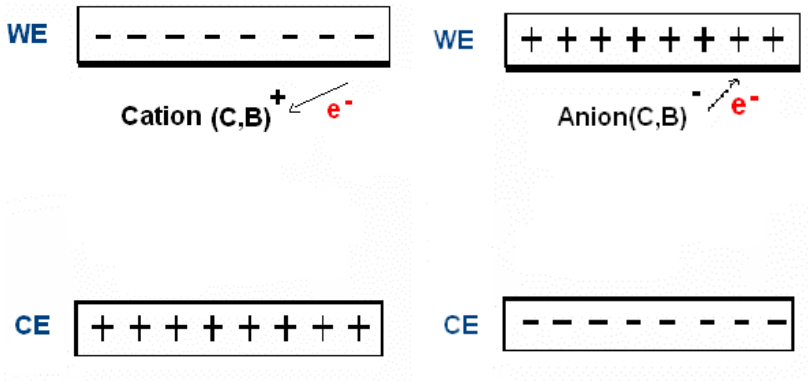

Figure 4.1. Schematic illustration of proposed electrochemical deposition of boron-doped diamond films

Due to the electrophoresis mechanism, the anion ions are also moving into the working electrode area and can be deposited on the substrates as boron-doped diamond films by

oxidation. If the organic compound is dissociated into carbon-containing cation/anion ion and boron-containing anion/cation ion respectively, a positive potential and negative potential will be alternatively applied into the working electrode. Then carbon atom and boron atom can be alternatively deposited on the substrates and finally form boron-doped diamond films. A schematic illustration of this proposed electrochemical deposition is shown in Figure 4.1.

In all, electrochemistry has demonstrated a great potential in the deposition of carbon films as a novel methodology. It is both rewarding and interesting to conduct more research in this field and further extend its application into the deposition of other thin films.

References

54. G. M. Swain and R. Ramesham, The Electrochemical Activity of Boron-Doped Polycrystalline Diamond Thin Film Electrodes, Anal. Chem., 65 (**1993**) 345.

55. S. Alehashem, F. Chambers, J. W. Strojek, G. M. Swain and R. Ramesham, Cyclic Voltammetric Studies of Charge Transfer Reactions at Highly Boron-doped Polycrystalline Diamond Thin-Film Electrodes, Anal. Chem., 67 (**1995**) 2812.

56. M. Boukezzata, D. Bielle-Daspet, G. Sarrabayrouse and F. Mansour, Characteristics of the Thermal Oxidation of Heavily Boron-doped Polycrystalline Silicon Thin Films, Thin Solid Films, 279 (**1996**) 145.

57. J. Xu, M. C. Granger, Q. Chen, T. E. Lister and G. M. Swain, Boron-Doped Diamond Thin-film Electrodes, Analytical Chemistry News & Features, October 1 (**1997**) 591 A.

58. L. Boonma, T. Yano, D. A. Tryk, K. Hashimoto and A. Fujishima, Observation of Photocurrent from Band-to-Band Excitation of Semiconducting p-Type Diamond Thin Film Electrodes, J. Electrochem. Soc., 144 (**1997**) L142.

59. J. Gaze, N. Oyanagi, I. Yamamoto and H. Izawa, Laser Ablation Doping Process for the Synthesis of Conductive Diamond Thin Film, Thin Solid Films, 322 (**1998**) 28.

60. Y. V. Pleskov, Y. E. Evstefeeva, M. D. Krotova, V.V. Elkin, V. M. Mazin, V.Y. Mishuk, V. P. Varnin and I.G. Teremetskaya, Synthetic Semiconductor Diamond Electrodes: The Comparative Study of the Electrochemical Behaviour of Polycrystalline and Single Crystal Boron-doped Films, Journal of Electroanalytical Chemistry, 455 (**1998**) 139.

61. S. Morooka, T. Fukui, K. Semoto, T. Tsubota, T. Saito, K. Kusakabe, H. Maeda, Y. Hayashi and t. Asano, Diamond and Related Materials, 8 (**1999**) 42.

62. L. L. G. Silva, M. K. Franco, F. Yokaichiya, N. G. Ferreira and E. J. Corat, Synchrotron Radiation X-ray analysis of Boron-Doped Diamond Films Grown by Hot-filament Assisted Chemical Vapor Deposition, Diamond and Related Materials, 11 (**2002**) 153.

APPENDIX A

Table 1. Experimental parameters for different samples, which were run by three-electrode system as discussed in chapter 2.

Number	WE	CE	D_1*	D_2*	E(V)	I(mA)	Q(C)	T(°C)	Time
7302001	brass	Ni-Cr	5 mm	13 mm	9.55-6.35	-0.50 ~ -0.16	-4.833	-60 ~ -50	5.2 h
8022001	brass	Ni-Cr	4 mm	14 mm	9.80-4.71	-0.50 ~ -0.10	-5.175	-65 ~ -60	6.5 h
3312001	Co	Pt	N/A	N/A	9.60-4.00	-0.40 ~ -0.10	-3.278	-42 ~ -37	5.3 h
6042001	Co	Pt	N/A	N/A	6.50-1.40	-0.50 ~ -0.05	-4.433	-58 ~ -52	5.0 h
6122001	Co	Ni-Cr	N/A	N/A	9.90-5.80	-0.50 ~ -0.07	-2.511	-60 ~ -50	4.8 h
4092001	Cu	Pt	N/A	N/A	4.00-1.80	-0.50	-10.19	-45 ~ -37	6.5 h
5312001	Cu	Pt	N/A	N/A	9	-1.90 ~ -0.65	-10.66	-55 ~ -50	3.0 h
6012001	Iron	Pt	N/A	N/A	9.00-5.00	-0.59 ~ -0.25	-4.523	-55 ~ -50	3.6 h
6142001	Mo	Ni-Cr	3 mm	8 mm	9.40-4.50	-0.40	-7.879	-60 ~ -50	5.5 h
7102001	Mo	Ni-Cr	3 mm	10 mm	9.61-6.89	-0.50 ~ -0.35	-9.094	-50 ~ -40	6.3 h
2062001	Ni	Pt	N/A	N/A	4.50-1.70	-1.00 ~ -0.35	-10.69	-55 ~ -50	6.5 h
2272001	Ni	Pt	N/A	N/A	5.00-1.40	-2.00 ~-0.30	-8.173	-70 ~ -65	2.8 h
2282001	Ni	Pt	N/A	N/A	4.00-1.40	-0.66 ~ -0.03	-3.517	-72 ~ -66	5.2 h
3012001	Ni	Pt	N/A	N/A	6.00-2.20	-2.20 ~ -0.10	-8.704	-65 ~ -40	4.4 h
4252001	Ni	Pt	N/A	5 mm	9.60-4.40	-0.50 ~ -0.20	-5.327	-54 ~ -48	4.0 h
4302001	Ni	Pt	N/A	N/A	9.00-6.60	-0.50 ~ -0.10	-1.899	-70 ~ -60	1.7 h
5012001	Ni	Pt	N/A	10 mm	9	-0.90 ~ -0.10	-3.322	-70 ~ -50	3.6 h
6072001	Ni	Ni-Cr	5 mm	10 mm	9.40-6.50	-0.40 ~ -0.10	-3.424	-60 ~ -50	4.8 h
6192001	Ni	Ni-Cr	4 mm	9 mm	9.20-5.00	-0.50 ~ -0.25	-8.614	-60 ~ -50	6.0 h
6212001	Ni	Ni-Cr	2 mm	5 mm	9.54-6.33	-0.40 ~ -0.15	-5.882	-60 ~ -50	7.8 h

6282001	Ni	Ni-Cr	5 mm	10 mm	9.92-5.97	-0.40 ~ -0.10	-3.695	-55 ~ -50	6.9 h
7032001	Ni	Ni-Cr	13 mm	15 mm	9.45-6.59	-0.30 ~ -0.20	-5.361	-45 ~ -40	6.2 h
7052001	Ni	Ni-Cr	1 mm	11 mm	9.96-6.46	-0.40 ~ -0.15	-5.121	-55 ~ -50	6.3 h
7122001	Ni	Ni-Cr	2 mm	8 mm	9.53-6.04	-1.00 ~ -0.25	-8.897	-50 ~ -40	7.0 h
7162001	Ni	Ni-Cr	3 mm	11 mm	9.53-6.04	-0.40 ~ -0.08	-3.081	-60 ~ -50	5.4 h
7182001	Ni	Ni-Cr	1 mm	12 mm	9.50-6.89	-0.79 ~ -0.08	-3.464	-65 ~ -55	4.5 h
4232001	SS	Pt	N/A	N/A	7.30-2.30	-0.50 ~ -0.20	-5.09	-70 ~ -60	5.2 h
6082001	SS	Ni-Cr	5 mm	10 mm	9.40-5.60	-0.50 ~ -0.20	-5.323	-60 ~ -50	4.5 h
6262001	SS	Ni-Cr	2 mm	4 mm	7.72-4.84	-0.50 ~ -0.15	-10.71	-50 ~ -40	7.0 h

* D_1 is the distance between working electrode and reference electrode.

D_2 is the distance between working electrode and counter electrode.

Table 2. Experimental parameters for different samples, which were run by two-electrode system as discussed in chapter 3.

Number	WE	CE	D*	E(V)	I(mA)	T (?C)	Time
8072001	brass	Ni-Cr	5 mm	-30	1.50-0.10	-70 ~ -61	4.9 h
8302001	brass	Ni-Cr	3 mm	-30	2.30-0.12	-65 ~ -55	4.3 h
8062001	Mo	Ni-Cr	5 mm	-30	1.00-0.08	N/A	3.0 h
8132001	Mo	Ni-Cr	6 mm	-30	1.80-0.23	-65 ~ -60	4.3 h
8172001	Mo	Ni-Cr	5 mm	-30	1.30-0.25	-60 ~ -55	4.2 h
8092001	Ni	Ni-Cr	8 mm	-30	1.10-0.13	-62 ~ -54	5.1 h
8242001	stainless steel	Ni-Cr	3 mm	-30	1.50-0.19	-70 ~ -64	1.8 h
8272001	stainless steel	Ni-Cr	6 mm	-30	1.50-0.10	-65 ~ -55	4.1 h
9052001	stainless steel	Ni-Cr	6 mm	-30	1.50-0.35	-65 ~ -45	3.5 h

* D is the distance between working electrode and counter electrode.

APPENDIX B

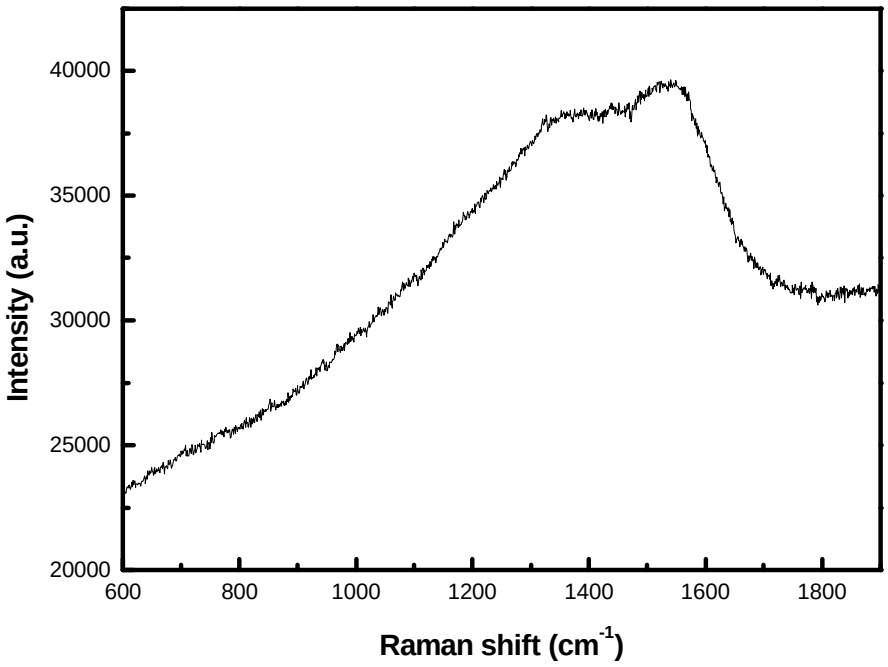

Figure 1. Raman spectra of Ni Sample 020601

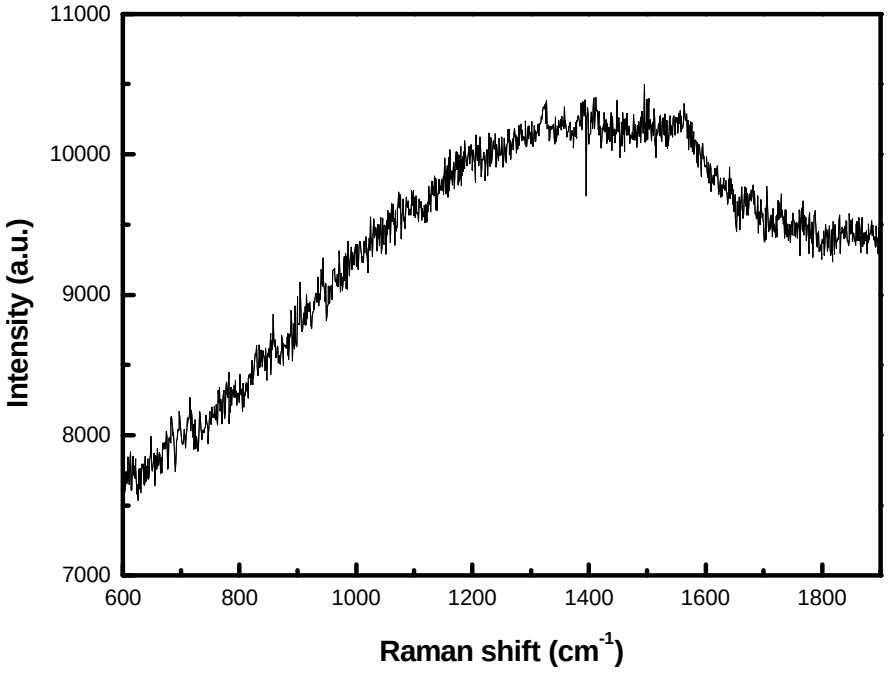

Figure 2. Raman spectra of Ni Sample 022701

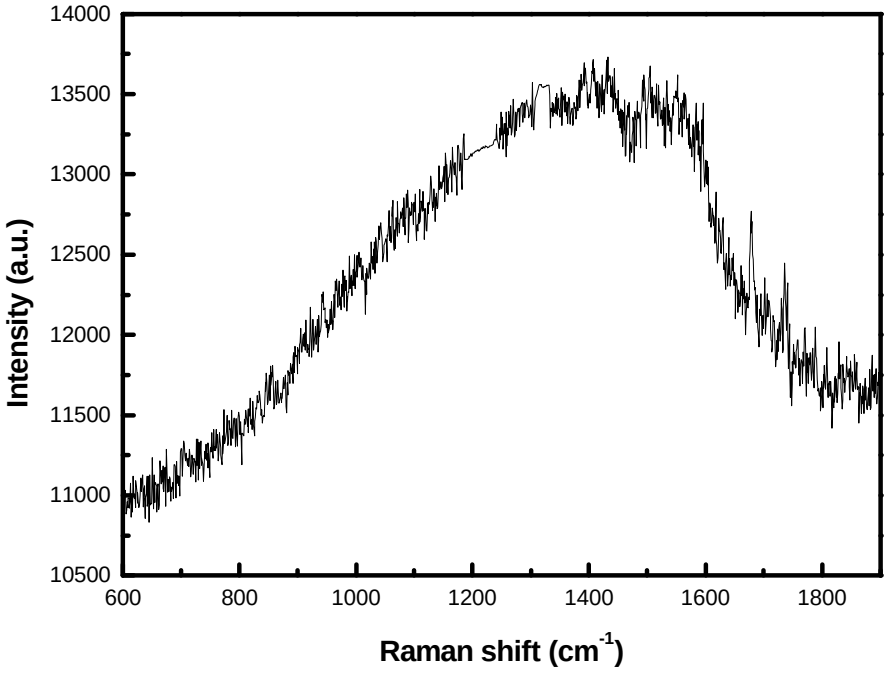

Figure 3. Raman spectra of Ni Sample 022801

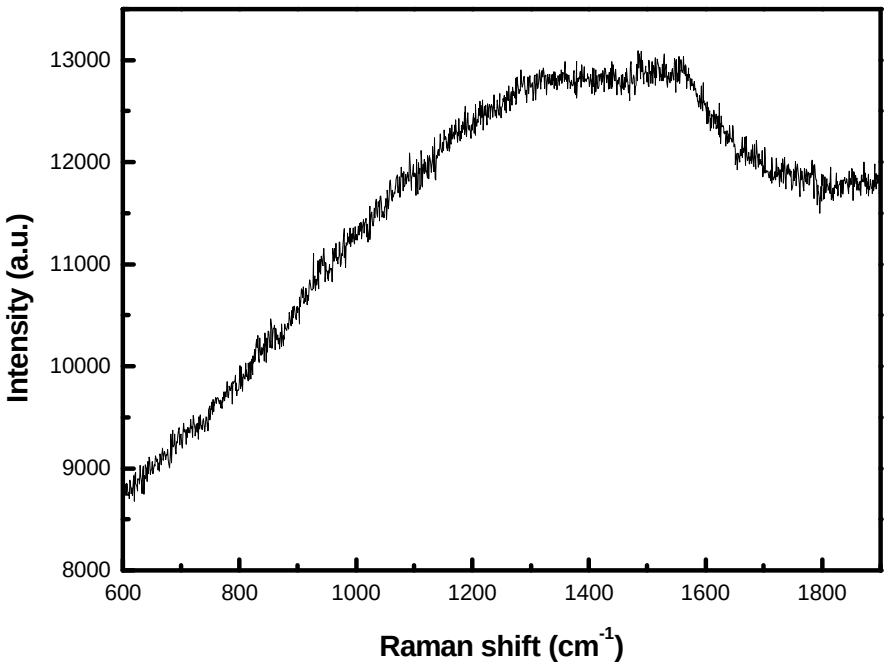

Figure 4. Raman spectra of Ni Sample 030101

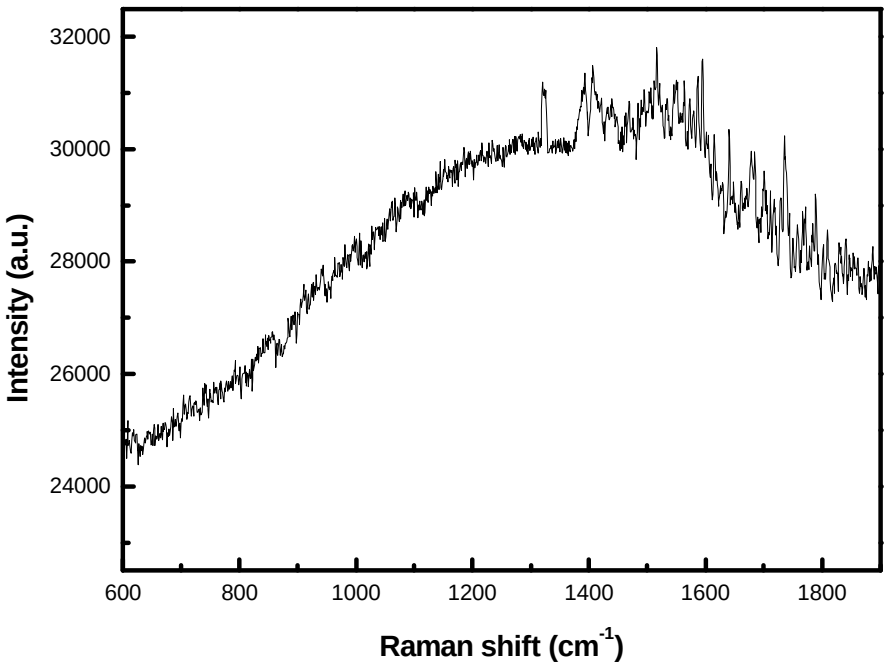

Figure 5. Raman spectra of Ni Sample 042501

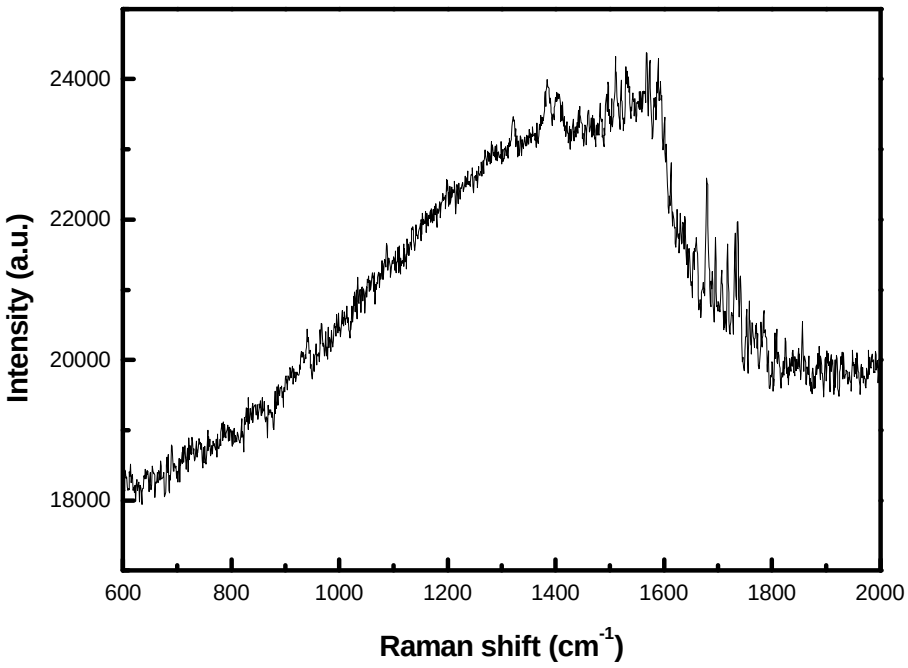

Figure 6. Raman spectra of Ni Sample 050101

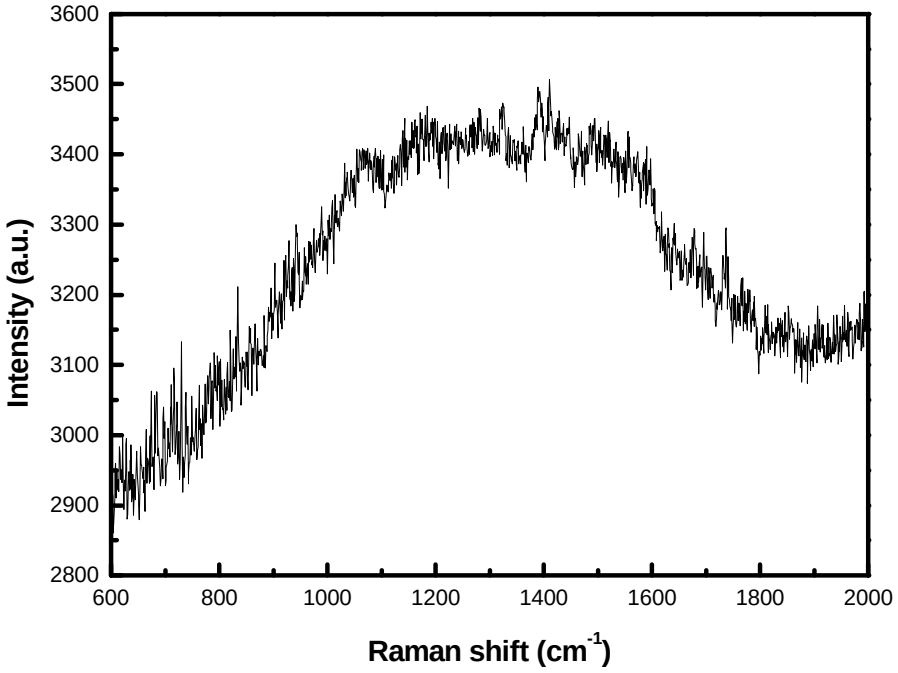

Figure 7. Raman spectra of Ni Sample 061901

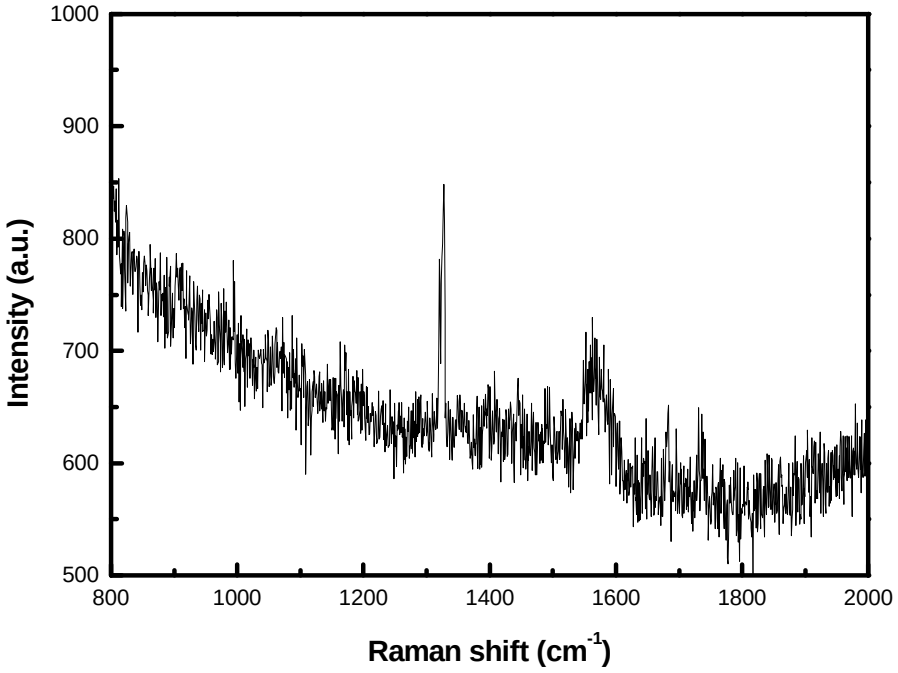

Figure 8. Raman spectra of Ni Sample 071801*

* The sharp peak at around 1332 cm^{-1} was found to be due to some instrumental error, but not diamond peak. When dealing with the Raman spectra, this sharp peak needs to be neglected.

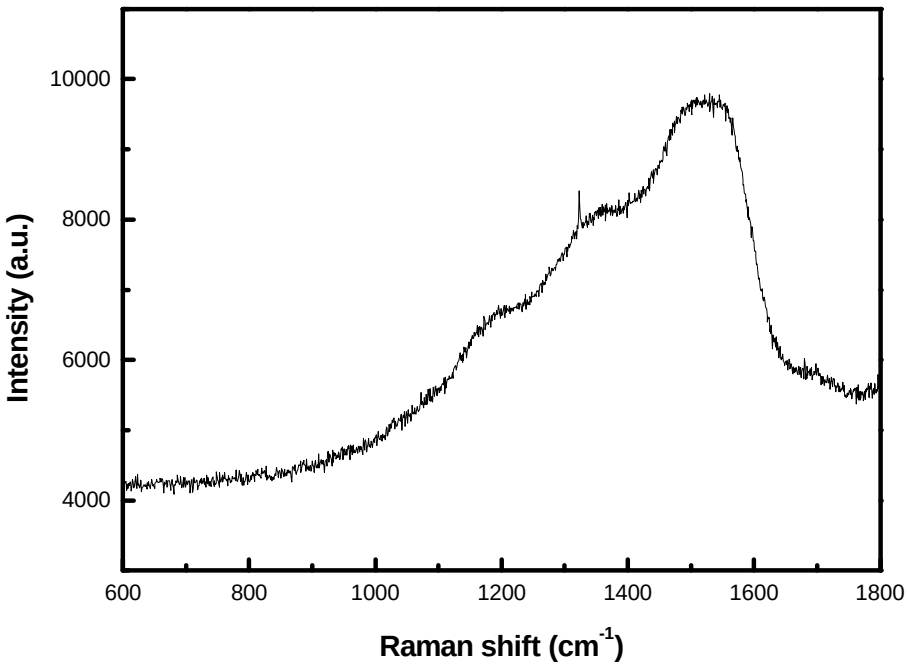

Figure 9. Raman spectra of Cu Sample 053101

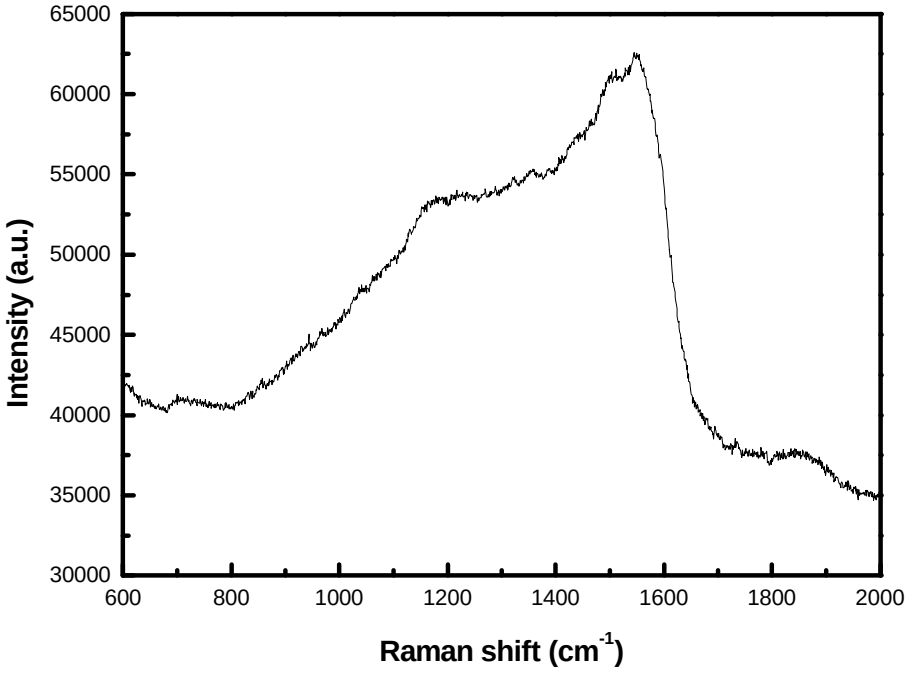

Figure 10. Raman spectra of Brass Sample 073001

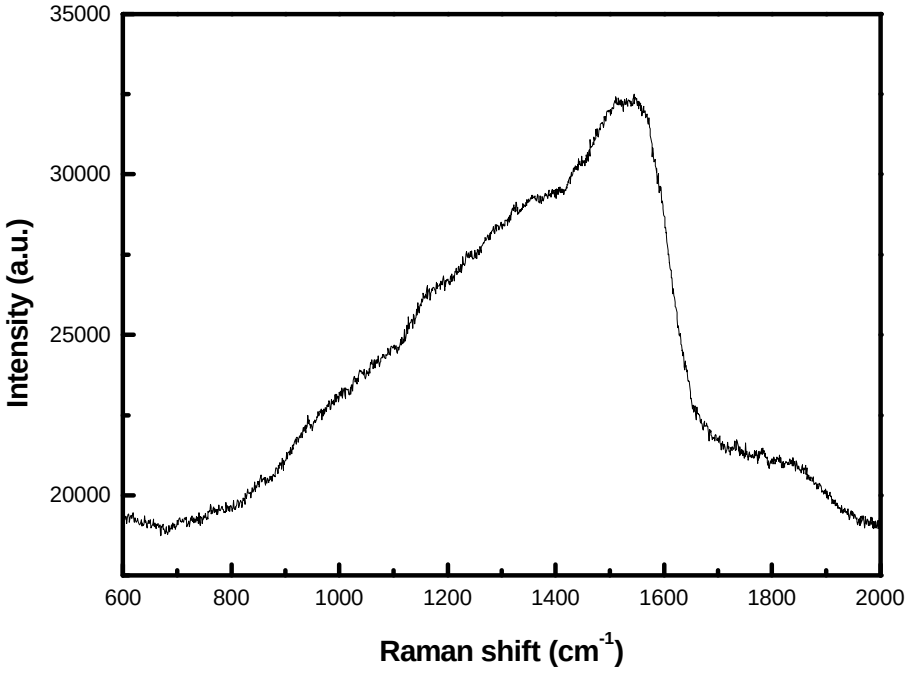

Figure 11. Raman spectra of Brass Sample 080201

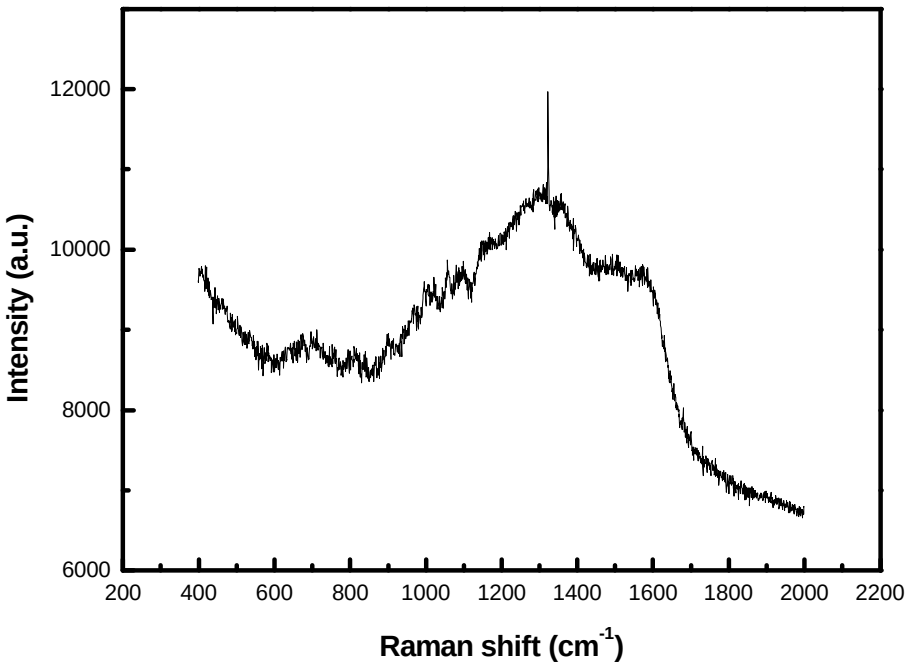

Figure 12. Raman spectra of Ni Sample 080901*

* The sharp peak at around 1332 cm^{-1} was found to be due to some instrumental error, but not diamond peak. When dealing with the Raman spectra, this sharp peak needs to be neglected.